Research Paper

THEMED ISSUE: Cenozoic Tectonics, Magmatism, and Stratigraphy of the Snake River Plain–Yellowstone Region and Adjacent Areas

GEOSPHERE

GEOSPHERE, v. 15,

https://doi.org/10.1130/GES01679.1

7 figures; 3 tables; 1 set of supplemental files

CORRESPONDENCE: katie.potter@usu.edu

CITATION: Potter, K.E., Champion, D.E., Duncan, R.A., and Shervais, J.W., 2019, Volcanic stratigraphy and age model of the Kimama deep borehole (Project Hotspot): Evidence for 5.8 million years of continuous basalt volcanism, central Snake River Plain, Idaho: Geosphere, https://doi.org/10.1130/GES01679.1.

Science Editor: Shanaka de Silva
Guest Associate Editor: Matthew E. Brueseke

Received 10 February 2018
Revision received 3 October 2018
Accepted 3 January 2019

GOLD OPEN ACCESS

THE GEOLOGICAL SOCIETY OF AMERICA®

This paper is published under the terms of the CC-BY-NC license.

© 2019 The Authors

Volcanic stratigraphy and age model of the Kimama deep borehole (Project Hotspot): Evidence for 5.8 million years of continuous basalt volcanism, central Snake River Plain, Idaho

Katherine E. Potter[1], Duane E. Champion[2], Robert A. Duncan[3], and John W. Shervais[1]

[1]Department of Geology, Utah State University, Logan, Utah 84321, USA
[2]Volcano Science Center, U.S. Geological Survey, 345 Middlefield Road, Menlo Park, California 94025, USA
[3]College of Earth, Ocean, and Atmospheric Sciences, Oregon State University, Corvallis, Oregon 97331, USA

ABSTRACT

The Snake River Plain of central Idaho represents the world's best example of a mantle hotspot track impinging upon continental crust and provides a record of bimodal volcanism extending over 12 Ma to the present. Project Hotspot recovered almost 2 km of continuous drill core from the Kimama borehole, located in central Idaho on the axial volcanic zone. The Kimama drill core represents the most complete record of mafic volcanism along the Yellowstone–Snake River Plain hotspot track.

A total of 432 basalt flow units, representing 183 basalt flows, 78 basalt flow groups, and 34 super groups, along with 42 sediment interbeds are recognized using volcanic facies observations, stratigraphic relationships, borehole geophysical logs, and paleosecular variation in magnetostratigraphy. Rhyolite and other non-basaltic volcanic materials were not encountered in the drill core.

Ages for six basalt lava flows were determined by $^{40}Ar/^{39}Ar$ using incremental heating experiments. Paleomagnetic inclination was measured on over 1200 samples collected at roughly 2-m-depth intervals, yielding mean values of paleosecular variation between ±50° to ±70° in Kimama flow groups, close to the expected 61° axial dipole average for the Kimama borehole location. Twenty-three magnetic reversals were identified and correlated to dated geomagnetic chrons and subchrons and compared with the $^{40}Ar/^{39}Ar$ radiometric ages. A linear fit to $^{40}Ar/^{39}Ar$ dates, geomagnetic chron and subchron boundaries, and volcanogenic zircon U-Pb ages defines a mean accumulation rate of ~320 m/m.y. and extrapolates to a bottom hole age of 6.3 Ma.

Average thicknesses of lithologic units increase from 2.7 m (sediment), 4 m (flow units), 10 m (flows), 23 m (flow groups), to 53 m (super groups). On average, one lava flow inundated the Kimama borehole location every 33 k.y. Intercalated sediments, ranging from 0.06 to 24.5 m thick, make up roughly 6% of the drill core and indicate lulls in local volcanic activity that may have lasted up to 77 k.y. Neutron and gamma-ray logs supplement observations from the drill cores: neutron logs document individual flow units through the contrast between massive flow interiors and more porous flow surfaces, and gamma-ray logs document the depth and thickness of sedimentary interbeds and high–K-Fe basalts. The 5.8 m.y. duration of basaltic volcanism in the Kimama drill core implies a steady rate of volcanism, indicating a relatively stable rate of mantle upflow along the lithosphere-mantle boundary in the wake of Yellowstone–Snake River Plain plume volcanism.

INTRODUCTION

Project Hotspot, the Snake River Scientific Drilling Project, was funded by the U.S. Department of Energy, the International Continental Drilling Program, and a consortium of universities. Three deep (1.8–1.9 km) boreholes were drilled in the central and western Snake River Plain (SRP) of Idaho (USA). The goals of the project were to document the history of hotspot volcanism in the wake of the Yellowstone plume, to understand how plume-related magmas interact with continental lithosphere, and to understand how this interaction affects the geochemical evolution of mantle-derived magmas and of the continental lithosphere. A further goal was to investigate innovative approaches to geothermal resource exploration in complex volcanic terranes (Shervais et al., 2011, 2012, 2013).

Although recent seismic tomography has imaged upper-mantle thermal and velocity anomalies beneath the Yellowstone–Snake River Plain (Y-SRP) volcanic province (Waite et al., 2006; Smith et al., 2009, Huang et al., 2015), obtaining a clear understanding of the source of hotspot magmatism and the extent of continental lithosphere interaction is only possible through the chemical analysis of erupted basalts. Of further importance is a record of these interactions through time as demonstrated by stratigraphic chemical variations and age constraints. Without basalt stratigraphy and the ability to assign chemical characteristics and ages to individual basalt flows, it is impossible to accurately determine either magmatic flux or the temporal source of chemical and isotopic heterogeneity related to the varying interaction between the continental lithosphere and a mantle hotspot source through time.

Investigations of stratigraphy in young continental volcanic provinces such as the SRP are restricted by the lack of uplift and tilting and by limited stratigraphic exposure in incised river canyons. As a result, detailed stratigraphic investigations in these terranes are limited by the depth and spatial distribution of cored wells (Shervais et al., 1994; Anderson et al., 1997). Many of the deeper

Downloaded from https://pubs.geoscienceworld.org/gsa/geosphere/article-pdf/doi/10.1130/GES01679.1/4663281/ges01679.pdf
by guest

wells in the SRP have been drilled to study groundwater and contaminant flow, and most are clustered on the Idaho National Laboratory (INL) site, located along the margin of the SRP north of the axial volcanic zone (AVZ) (Fig. 1). The Kimama drill site was chosen specifically to study the volcanic stratigraphy of the AVZ and to investigate elevated thermal gradients beneath the Snake River regional aquifer (Shervais et al., 2013; Lachmar et al., 2017).

The Kimama drill site is located in the AVZ of the central Snake River Plain (CSRP), ~21 km north of Burley, Idaho, and 65 km southwest of Craters of the Moon National Monument and Preserve at 270422 E and 4746659.6 N (UTM WGS 84, zone 12), 42.84°N, –113.81°W (latitude, longitude decimal degrees) (Fig. 1). The AVZ is a topographic high composed of tholeiitic shield volcanoes that represents the locus of basaltic volcanism during the late Pliocene and Pleistocene and is mirrored by a keel of buried basalts that has been documented in geophysical analyses (Lindholm, 1996). Previous drilling in other areas of the SRP has indicated a veneer of up to 1.2-km-thick Pliocene–Pleistocene basalt, with minor interbedded sediments of aeolian, fluvial, and lacustrine origin that overlie silicic volcanic products on the SRP (Doherty et al., 1979; Kuntz et al., 1992; Anderson and Liszewski, 1997).

The Kimama borehole was cored continuously from just below the surface (~12 m depth) to a total depth of 1912 m, with >99.5% recovery rate (length cored/core recovered); an additional 127 m of drill core was obtained as a result of a sidetrack that began in a sediment horizon at ~190–202 m depth (Kimama 1A). A second, more vertical wellbore (Kimama 1B) was drilled past the first borehole and duplicated 127 m of section as it continued to total depth. Kimama 1A encompasses core recovered from 13.4 m to 329 m depth, and core from Kimama 1B comprises core recovered from 202 m to total depth (T.D. 1912 m depth). Collectively, the Kimama drill core represents a nearly continuous record of volcanic activity and sedimentation at the Kimama site. Our approach to understanding the volcanic stratigraphy in the CSRP combines direct observation of drill core with information gained from wireline geophysical logs, paleomagnetic inclination range, depth, and correlations to the geomagnetic polarity time scale (Gradstein et al., 2012), radiometric ages, and geochemistry. In the absence of surface outcrops, drill-core data provide

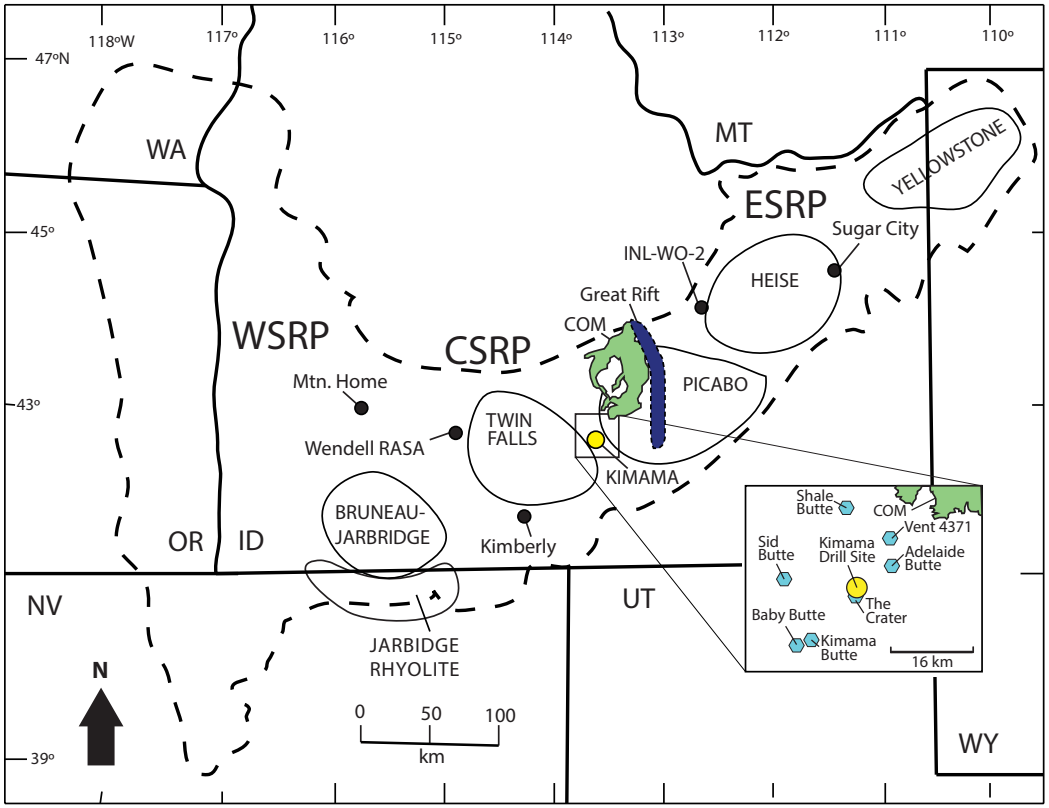

Figure 1. Location map showing regional geology including physiographic regions of the Snake River Plain, including the western Snake River Plain (WSRP), central Snake River Plain (CSRP), and the eastern Snake River Plain (ESRP) segments. The extent of the SRP region is outlined by the dashed line. The inferred locations of volcanic centers associated with the Yellowstone–Snake River Plain volcanic hotspot (after Anders et al., 2009), Craters of the Moon National Monument and Preserve (map notation: COM), and the Great Rift are distinguished by polygons. Several deep borehole and vent locations are delineated by black circles, including Mtn. Home, Wendell Regional Aquifer Systems Analysis (Wendell RASA), Kimberly, Idaho National Laboratory (INL-WO2), and Sugar City. The yellow dot signifies the location of the Kimama bore hole. The inset map shows the location of the Kimama drill site with respect to vents within a 16-km radius of the borehole. Seven vents, including Adelaide Butte, are exposed on the surface and are indicated by blue polygons. Distal flows from Craters of the Moon National Monument and Preserve are present in the NE corner of the inset map; the edges of these flows are ~20 km from the Kimama drill site. ID—Idaho; MT—Montana; NV—Nevada; OR—Oregon; UT—Utah; WY—Wyoming.

Downloaded from https://pubs.geoscienceworld.org/gsa/geosphere/article-pdf/doi/10.1130/GES01679.1/4663281/ges01679.pdf
by guest

our most direct record of the volcanic stratigraphy, flow contacts, flow characteristics, and sedimentary interbeds, as well as samples for geochemical and remanent magnetic analyses. Wireline geophysical logs may be used to supplement drill-core data, especially in situations where drill-core recovery is limited. In particular, gamma-ray and neutron logs are useful for interpreting basalt flows and interbedded sediments (Anderson and Lewis, 1989). As discussed below, gamma-ray logs are sensitive to sedimentary interbeds, whereas neutron logs document individual basalt flow units, especially when alteration makes the determination of original flow boundaries difficult. Thick packages of sediments (up to 24.5 m thick) demonstrate periods of volcanic quiescence of thousands of years, and/or climate variation, and bracket flow groups derived from a distinct magmatic source (typically from a single volcano).

Temporal information comes from variations in remanent magnetic inclinations (paleosecular variation), magnetic reversals, and radiometric age determinations. Minimal variations of a few degrees in magnetic inclination with depth document decade to multi-decade time scales, while significant inclination shifts and magnetic polarity reversals represent significant century to millennial-scale events (Champion et al., 1988). These variations can be used to distinguish individual basalt flows, which typically comprise multiple smaller flow units, and to identify packages of geochemically related flows, termed flow groups, which may be separated by differing inclination values and polarity. Radiometric dating of individual lava flows at critical depths not only provides direct information on ages and accumulation rates but also provides calibration of the paleomagnetic time scale, which can then be used to refine the stratigraphic age model. Trends in geochemical data (e.g., upsection cycles of increasing K_2O, TiO_2, Mg#, and total iron as FeO*, as well as ratios of Ti/K, La/Lu, and Zr/Nb) are used as a tool to identify individual flow groups (Shervais et al., 2006; Jean et al., 2013; Potter et al., 2018).

The ultimate goal of our research on the Kimama drill core is to merge lithologic observations and ages with major- and trace-element geochemistry and radiogenic isotope ratios to generate a complete history of basaltic volcanism in the CSRP. The integration of lithology, flow structures, wireline logs, magnetostratigraphy, all discussed here, and geochemistry, discussed in Potter et al. (2018), provides a powerful set of tools to interpret the timing, extent, and source of regional volcanism related to passage of the Yellowstone hotspot magmatism. The volcanic flux, and the volume of magma erupted through time, are first-order constraints on the ultimate origin of the hotspot and on its interaction with continental lithosphere. These calculations will rely critically on the stratigraphic and age models that we develop here.

GEOLOGIC BACKGROUND

Regional Setting

The 500-km-long central and eastern segments of the SRP formed as North America passed over the relatively fixed Y-SRP hotspot during the late Neogene. As the archetype of a continental hotspot track, the SRP contains a continuous record of often violent, episodic caldera-forming eruptions and quiescent basaltic volcanism (Morgan, 1972; Armstrong et al., 1975; Pierce and Morgan, 1992, 2009; Smith and Braile, 1994). A typical sequence of continental plume volcanism begins with intrusions of mafic, plume-derived magmas that drive the melting of continental lithosphere. Eruptions of silica-rich rhyolitic magmas occur over 2–4 m.y., after which the continental lithosphere is sufficiently depleted to allow the eruption of mantle-derived basalts (Jean et al., 2018; Shervais et al., 2014). The sequence of rhyolite, basalt, and sedimentary rocks that comprise the SRP spans 17 m.y. of volcanic activity (Fig. 2).

During the Pliocene through Pleistocene, the SRP was the locus of numerous mafic volcanic centers along the hotspot track that erupted thick packages of basalt flows. This volcanic activity was concentrated along the central axis of the plain to form the AVZ (Hackett and Smith, 1992; Hackett et al., 2004). Holocene lavas (e.g., the Shoshone lava flow and Craters of the Moon lava field) erupted on the margins of the plain. Other eruptions, such as the Great Rift, formed volcanic rift zones that cross the plain at high angles and are inferred to be derived from preexisting Basin and Range structures (Kuntz et al., 2002). Late Pleistocene to Holocene lavas of Craters of the Moon formed multi-phase polygenetic eruptions with ^{14}C ages of 2030 ± 80–11,000 ± 100 yr B.P. (Kuntz et al., 1986, 2007; Bonnichsen and Godchaux, 2002; Putirka et al., 2009).

Basalt Flow Stratigraphy

The monogenetic, or single-pulse eruptive episodes common on the SRP are similar to modern volcanic processes on the island of Hawaii and transitional between Hawaiian-style and continental-style volcanism (Fig. 2) (Kuntz, 1978; Greeley, 1982). Volcanic rift zones and low shield volcanoes erupted olivine tholeiite basalt lavas, filling subsiding basins and controlling the direction and deposition of subsequent lava and stream flow. During periods of decreased volcanism, lava flows were mantled by aeolian loess or fluvial sediments. Loess deposition can occur relatively quickly, although preservation is variable and short-lived (Kuntz et al., 1986, 1992). SRP shield volcanoes are typically low-slope due to fluid lavas and modest (±100 m) accumulation of lava near the vent, and they are recognized as being the product of small, mid-crustal magma chambers (Kuntz et al., 1986; Hon et al., 1994; Hughes et al., 1999, 2002). Eruptions were of relatively short duration, and low-viscosity basalt lava was efficiently transported away from the vent in inflated, endogenous-fed pahoehoe flows (Self et al., 1998; Champion et al., 2011). This type of volcanism has been described as "plains-style volcanism" by Greeley (1982).

As a result of "plains-style" eruptive processes and flow mechanisms, the classification of multiple assemblages of lava flows is scale dependent. Basalt flows are classified as either simple or compound lava flows, depending on whether the flow consists of a single coherent flow unit or an amalgamation of many thinner flow units (Walker 1971, 1991, 1993). Compound flows typically comprise stacks of relatively thin pahoehoe flows with or without an

Downloaded from https://pubs.geoscienceworld.org/gsa/geosphere/article-pdf/doi/10.1130/GES01679.1/4663281/ges01679.pdf
by guest

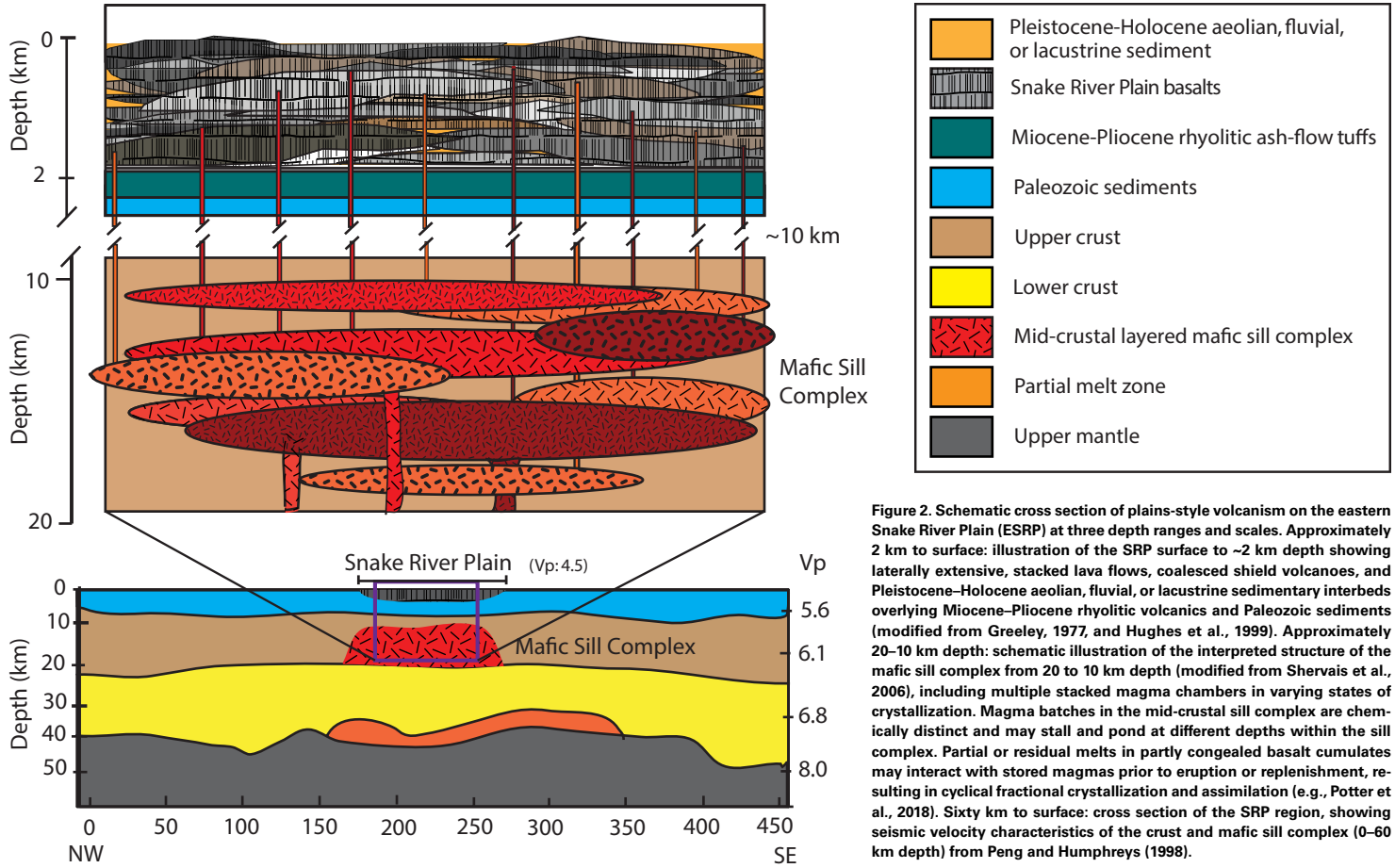

Figure 2. Schematic cross section of plains-style volcanism on the eastern Snake River Plain (ESRP) at three depth ranges and scales. Approximately 2 km to surface: illustration of the SRP surface to ~2 km depth showing laterally extensive, stacked lava flows, coalesced shield volcanoes, and Pleistocene–Holocene aeolian, fluvial, or lacustrine sedimentary interbeds overlying Miocene–Pliocene rhyolitic volcanics and Paleozoic sediments (modified from Greeley, 1977, and Hughes et al., 1999). Approximately 20–10 km depth: schematic illustration of the interpreted structure of the mafic sill complex from 20 to 10 km depth (modified from Shervais et al., 2006), including multiple stacked magma chambers in varying states of crystallization. Magma batches in the mid-crustal sill complex are chemically distinct and may stall and pond at different depths within the sill complex. Partial or residual melts in partly congealed basalt cumulates may interact with stored magmas prior to eruption or replenishment, resulting in cyclical fractional crystallization and assimilation (e.g., Potter et al., 2018). Sixty km to surface: cross section of the SRP region, showing seismic velocity characteristics of the crust and mafic sill complex (0–60 km depth) from Peng and Humphreys (1998).

underlying core of massive basalt representing an earlier syneruptive flow unit. In contrast, simple lava flows typically comprise a massive flow unit with a shelly or rubbly upper surface. In either case, the lava flow is considered to represent a single eruptive event formed over a time scale of weeks to years, but commonly less than a few decades (Kuntz et al., 1992; Champion et al., 2011).

Late Pleistocene–Holocene basaltic lava fields within the SRP display volcanic features analogous to those found in modern lava flows such as those exposed in low-slope areas of Kilauea and Mauna Loa volcanoes in Hawaii (Hon et al., 1994). Pahoehoe flows produce complex stratigraphy with younger eruptions of lava conducted away from the vent through the molten interiors of older flow units, a process involving inflation of the surface as lavas continue to be erupted from the vent (Walker 1991; Chitwood, 1994; Self et al., 1998). Therefore, the massive core of a flow represents the last or a late-stage pulse of an eruption, while the shelly and rubbly surface and basal facies represent marginally earlier time frames of the same eruption. With regard to drill core, inflation dictates that younger flow units may be bounded at top and bottom by relatively older basalt flow units from the same eruption, an observation that has important implications for stratigraphic interpretation. Self et al. (1998) recognized that the inflation mechanism of pahoehoe flows produces lavas that display similar geometries at variable spatial scales. Flow units represent the smallest scale lava assemblage and are analogous to flow lobes produced during inflation processes. Lava flows are slightly larger assemblages with

Downloaded from https://pubs.geoscienceworld.org/gsa/geosphere/article-pdf/doi/10.1130/GES01679.1/4663281/ges01679.pdf
by guest

greater thickness and areal coverage. Both flow units and flows draw from the same magma reservoir but may erupt during all phases of a monogenetic eruption from a vent (or vents) tapping into a unique magma reservoir (Fig. 2). Packages of flow units and flows that erupt from a single magma reservoir over its lifespan will form larger-scale assemblage, a complex aggregate of lavas termed "flow groups" (Fig. 3A) (Hughes et al., 2002; Welhan et al., 2002). Flow groups have areal dimensions of one to tens of square kilometers and are analogous to lava fields, such as the Wapi and Hell's Half Acre lava fields (Fig. 3B) (Greeley, 1982; Welhan et al., 2002). Super groups encompass coeval eruptions from multiple magma systems and typically contain several geochemically unrelated flow groups of the same magnetic polarity, e.g., flow groups at Craters of the Moon National Monument and Preserve (Hughes et al., 2002).

When discussing volcanic stratigraphy, however, it is important to note that the processes of basaltic volcanism make data from a single drill core an imperfect record of eruptive activity and hiatus. Continuous lava flow inundation on a sector of a flank of a volcano may occur while another sector remains unaffected. Similarly, a dormant volcano may be inundated by lavas from an adjacent volcano. In addition, interfingering of lava flows from adjacent volcanoes may occur if eruptive activity is simultaneous (Jean et al., 2013). SRP volcanism creates constructional topography in which topographic highs represent volcanic constructs (not erosional remnants), drainage patterns are determined by the distribution of volcanic constructs, and older, extinct vents are buried progressively by flows from nearby active vents. Although the Kimama drill core contains a record of eruptions from dozens of magmatic events, only seven vents are preserved in a 16-km radius around the drill site (Fig. 1). This is not unique on the CSRP, where most older vents have been obscured by weathering and erosion or newer lava flows. In contrast, the eastern SRP (ESRP) has a much greater concentration of exposed vents—likely due to their younger age.

Accumulation rates of SRP basalt volcanism are averaged over hundreds of thousands of years to account for hiatuses due to vent construction, periods of decreased volcanism, differential subsidence, and uplift (Anderson and Liszewski, 1997; Anderson et al., 1997). Each lava flow group encountered in drill core generally represents a time period of volcanic activity no longer than a few hundred years; whereas, a sedimentary interbed or significant change in paleomagnetic inclination can represent thousands to tens of thousands of years of volcanic inactivity. This is sufficient time to allow deposition of thick and thin layers of sediment and for the Earth's geomagnetic field to undergo secular variation and possible polarity change (Champion et al., 1988; Anderson et al., 1997).

METHODS

Lithologic Logging

Detailed lithologic logging was accomplished through physical observations of drill core and through the use of high-resolution drill-core photographs. Basalt drill core was visually inspected for large-scale features such as fractures, oxidation or scoriaceous regions, sediment interbeds, megavesicles, vesicle-rich zones (vesicle sheets, vesicle bands, or vesicle cylinders), pillows, and rubble zones, as well as smaller-scale features including ropey flow tops, flow and mold structures, and spatter. Drill-core samples displaying alteration, oxidation, secondary mineralization, xenoliths, autoliths (syneruptive lava fragments emplaced in the lava flow), anomalous vesiculation, and other distinguishing characteristics were described when observed.

We identified flow unit boundaries throughout the entire 1912 m of Kimama drill core using the model of Self et al. (1998), who suggest that individual pahoehoe lava flows and their constituent flow units display three distinctive zones: surface, interior, and basal facies (Fig. 4A). Modern volcanic features provide a tangible corollary to aid in the identification of subsurface features in the drill core.

Surface Facies

The flow surface is characterized by oxidized, platy or rubbly, and highly vesicular textures, often with ropey morphology (Figs. 4B and 4C). Stacks of multiple surface facies are occasionally observed, with washed-down sediment coatings on surface facies forming simple boundaries (Fig. 4D). Surface facies thicknesses range from 30 cm to 1 m. When flow lobes succeed one another without sufficient time separation, new flow lobes may make molds of the underlying flow surface as they cool, creating "flow and mold structures" (Twining et al., 2008) or flow molds (Hodges, 2010, personal commun.) (Fig. 4E).

The transition from surface facies to interior facies is observed as near-surface vesicle bands, or segregation veins, visible as submillimeter-sized vesicles within fine-grained crystalline basalt (Fig. 4F). Depressurization during flow lobe breakout causes a pulse of vesiculation in the liquid lava, which eventually cools into a horizontal vesicle layer (segregation vein) (Hon et al., 1994). Multiple, stacked segregation veins, without chilled margins, may be present within a single lava flow and are a principal facies indicator of inflated pahoehoe flows (Smith, 1967; Walker, 1993; Chitwood, 1994; Self et al., 1998; Welhan et al., 2002).

Interior Facies

Flow interiors commonly exceed three meters in thickness and are characterized by massive fine-grained intersertal or intergranular textures. Because thicker flows take longer to solidify, their interiors typically have near-complete loss of vesicles from the lower and middle portions and are described as "massive basalt" (Fig. 4G) (Walker, 1993). Coarser-grained diktytaxitic textures with isolated vesicle structures including vesicle pipes, macrovesicles, and segregation veins are also commonly observed. Diktytaxitic texture (Fig. 4H), vesicle pipes (Fig. 4I), macro vesicles (Fig. 4J), and vesicle segregation veins,

Downloaded from https://pubs.geoscienceworld.org/gsa/geosphere/article-pdf/doi/10.1130/GES01679.1/4663281/ges01679.pdf
by guest

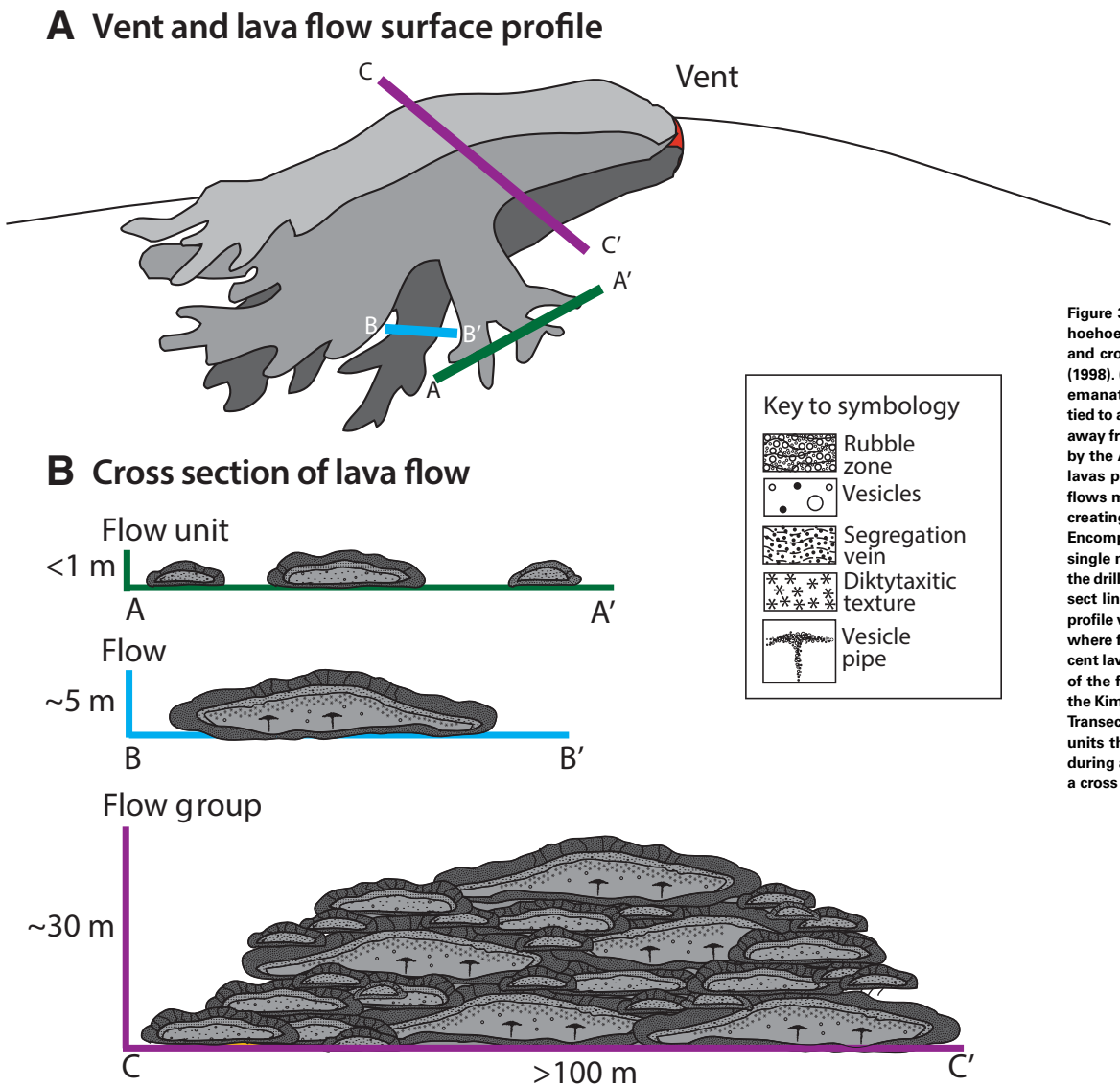

Figure 3. Spatial relationship between inflated pahoehoe flow units, flows, and flow groups in map and cross section views, modified from Self et al. (1998). (A) Profile of a flow field showing lava flows emanating from a vent during a magmatic event tied to a single reservoir (Kuntz et al., 1992). Farthest away from the vent is the flow front (flow unit), cut by the A–A′ transect line. Moving toward the vent, lavas progressively thicken into flows, and older flows may be blanketed by newer flows over time, creating a flow group, indicated by transect B–B′. Encompassing all flows and flow units erupted from single magma reservoir, flow fields (represented in the drill core as flow groups) are cut by the C–C′ transect line. (B) Cross sections of transects shown in profile view: transect A–A′ illustrates the flow front, where flow lobes (flow units) advance as incandescent lava oozes through the cooled rind at the edge of the flow. The average thickness of flow units in the Kimama drill core ranges from 1.17 m to 9.75 m. Transect B–B′ illustrates the lava flow, where flow units thicken by inflation as they extend outward during a volcanic eruption. Transect C–C′ illustrates a cross section of a lava flow group.

Downloaded from https://pubs.geoscienceworld.org/gsa/geosphere/article-pdf/doi/10.1130/GES01679.1/4663281/ges01679.pdf
by guest

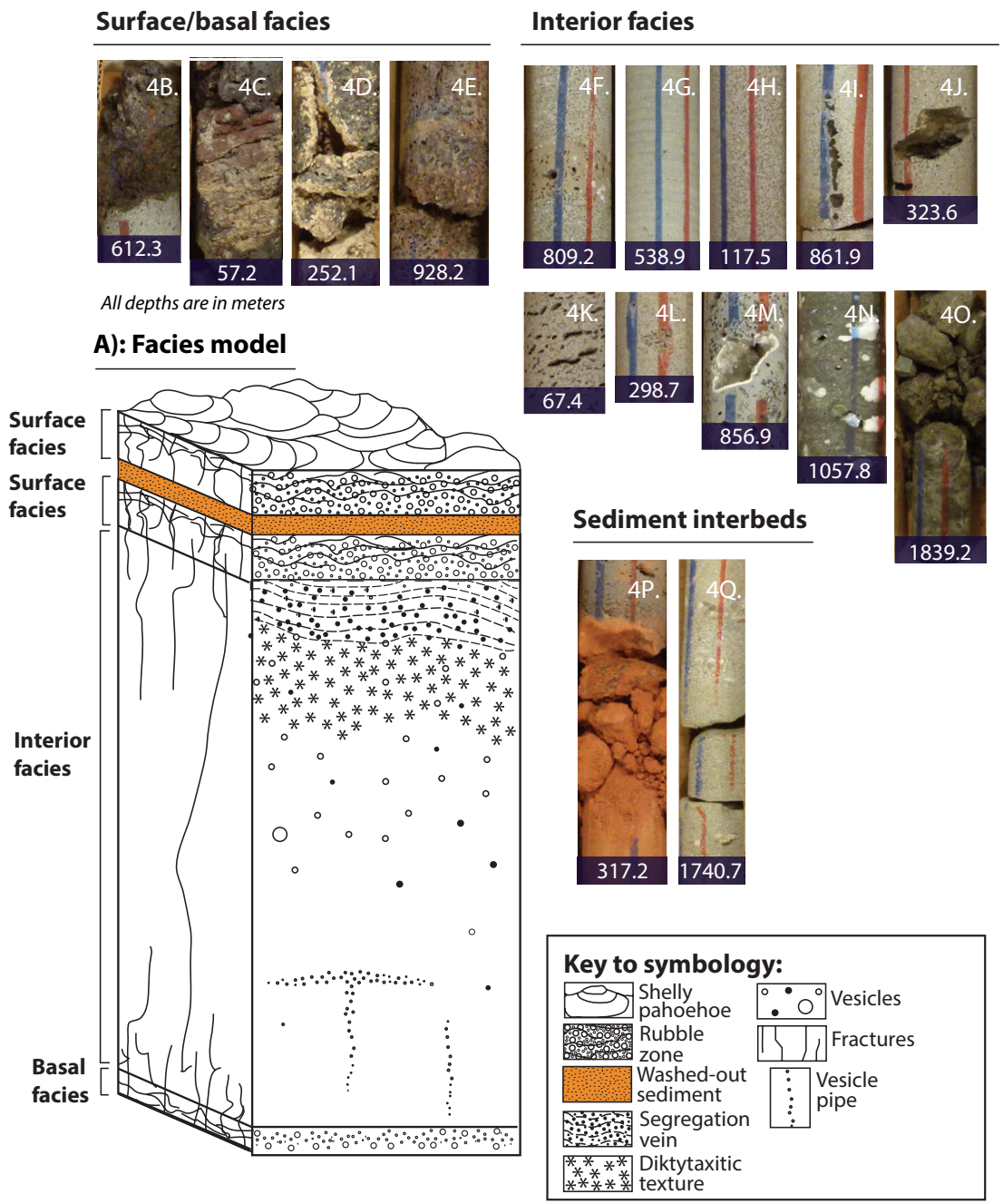

Figure 4. (A) Schematic illustration of a typical (~6.2 m) inflated simple basalt flow as observed in the Kimama drill core, modified from Self et al. (1998). (B–Q): Photographs and depths of flow facies in the Kimama drill core. The depth of recovery in meters is given at the base of each photograph. Surface facies: glassy spatter (B), ropey pahoehoe (C), sediment-coated rubble (D), and flow and mold structures (E). Interior facies: segregation veins (F); massive flow interior, without vesicles (G); diktytaxitic texture (H); vesicle pipe (I); macrovesicle (~5 cm across) (J); elongate vesicles, a result of continued lava flow during cooling (K); remobilized spatter (also referred to as autolithic basalt) (L); calcite amygdule (M); smectite amygdule (N) (after Sant and Shervais, 2011); and hyaloclastite (O). Sediment interbed characteristics vary through the drill core: baked loess, fine-grained homogenous clay baked to terra cotta by the overlying lava flow (P); fluvial sediment interbed with normal grain-size gradation (detrital zircon samples were obtained from fluvial sediment layers at the base of the core for U-Pb analyses) (Q); and sediment-coated rubble (D).

Downloaded from https://pubs.geoscienceworld.org/gsa/geosphere/article-pdf/doi/10.1130/GES01679.1/4663281/ges01679.pdf
by guest

also present in the transition zone facies, are thought to be a product of cyclic vesiculation, or repeated cycles of lava flow inflation and gas exsolution during flow breakout (Goff, 1996; Hughes et al., 2002). Diktytaxitic texture indicates secondary exsolution and is characterized by lath-like clusters of plagioclase bounding sub-mm vesicles. Pipe vesicles form near the base of the lava flow at the crystallization front. The characteristic umbrella shape is a result of vesicular residuum rising slowly through stagnant lava to the base of the upper cooling surface, where the residuum spreads laterally and forms horizontal vesicle sheets (Self et al., 1998).

Elongate vesicles (Fig. 4K) indicate ductile deformation gas bubbles trapped in partially solidified lavas during inflation and flow. Dense clusters of vesicles surrounded by fine-grained basalt are thought to be remobilized spatter (autoliths) (Fig. 4L). Carbonate clay commonly coats basalt rubble zones within the ~250-m-depth vadose zone, and at depths greater than ~900 m, secondary alteration is evident in basalt flows sampled from depths of 850–1912 m. A gradation of alteration ranging from calcite amygdules at depths of ~850 m (Fig. 4M) to Smectite, and montmorillonite amygdules (Fig. 4N) below 900 m demonstrates the effects of increased heat flow with greater depth (Sant, 2013; Lachmar et al., 2017). The alteration of interstitial glass to clay minerals and the iddingsitization of olivine phenocrysts signal pervasive alteration below 1300 m depth (Sant, 2013). Evidence of the interaction of basalt and water is found below 1750 m depth as highly altered hyaloclastite (4O).

Individual flow units almost invariably transition from darker-gray basalt in the upper and lowermost portions of the flow unit to lighter gray within the interior, indicating a greater content of groundmass glass in the more rapidly cooled upper and lower portions. Vesicles, always subrounded to rounded, display a trend of increased size and decreased frequency upward to the flow interior, at which vesiculation largely ceases. Above the flow interior, the concentration of vesicles increases and vesicle size decreases through the top of the flow unit. Missing intervals (unrecovered drill core) between flow groups are usually associated with rubbly sections (Fig. 4D) or sediment interbeds (Figs. 4P and 4Q), both of which are easily disturbed by drilling.

Basal Facies

The flow unit base contains minor vesiculation and may contain rubble. In the Kimama drill core, the basal lava flow unit facies occur in thicknesses generally less than 5 cm. Degassing is most efficient in the lower portion of the flow unit, resulting in relatively minor vesiculation in the basal facies relative to the interior and surface facies. A thin, >2 cm rind of glass often designates the chilled contact of the lava flow unit with the ground surface.

Significant time separation between eruptive events is sometimes indicated by the presence of fine-grained to coarse-grained sediments from aeolian and fluvial sources. Sediments collect in topographically low (fluvial) or leeward settings (aeolian). The Kimama drill core contains both types of sediment, but in a strict bimodal distribution. Loess deposits are exclusively found above 1730 m depth (Fig. 4O) in the Kimama drill core, while fluvial sediments (Fig. 4P) are entirely absent until below 1730 m depth. Aeolian sediments lack internal structure or depositional facies, but fluvial sediments in Kimama drill core typically contain fining-upward bedding. In some cases, sediment layers may have been baked by overlying lava flows (Fig. 4O; baked loess).

As a result of weathering and water movement, sediment-filled vesicles are most common within flow units that are immediately beneath sediment interbeds. One interval between 1750 and 1882 m depth preserves the interaction of lava, water, and sediment as hyaloclastite deposits; these deposits have been heavily altered by thermal waters (Sant, 2013; Lachmar et al., 2017).

Wireline Geophysical Logging

Wireline geophysical logs for both boreholes (Kimama 1A and 1B) were made in stages as drilling progressed, with the final logging shortly after completion of borehole 1B. The upper ~760 m were logged by the U.S. Geological Survey using tools and techniques described in Twining and Bartholomay (2011). Borehole 1A was logged in October 2010 (0–298 m depth). Borehole 1B was logged in November 2010 (0–759 m). Logs for both boreholes included natural gamma ray, neutron, gamma-gamma density, temperature, and gyro deviation. Century Wireline Services performed neutron and natural gamma-ray log measurements in January 2011; these measurements were made inside the drill string in order to avoid tool loss (206–1850 m); caliper, natural gamma-ray, sonic porosity, resistivity, self-potential, and temperature logs were measured in the open hole below the HQ drill string. Temperatures in the lower 100 m of the borehole exceeded the limits of the instruments, resulting in electronic noise below ~1800 m depth. Final logging was carried out by the Operational Support Group (OSG) of the International Continental Drilling Program (GeoForschungsZentrum [Geo-research Centre (GFZ)-Potsdam]. These included natural gamma, spectral gamma, magnetic susceptibility, electrical, resistivity, borehole, sonic, dip meter, and borehole televiewer logs measured in the open hole below the HQ drill string; a blockage in the hole at ~1408 m prevented deeper open hole logging.

In SRP boreholes, natural gamma rays are emitted primarily by ^{40}K-bearing clays, which are concentrated in the sedimentary interbeds. Gamma-ray logs are thus the primary tool for determining the presence of sediment interbeds, and by association, stratigraphic breaks between basalt flow groups. Furthermore, natural gamma-ray logs may be used to identify individual basalt flows should they contain measurable differences or relative abundances in K_2O concentration (Twining et al., 2008). In general, sedimentary interbeds are characterized by high natural gamma-ray signals relative to the surrounding tholeiitic basalts. However, several high K_2O basalt lavas are characterized by moderately high gamma-ray signals (higher than the tholeiitic basalts and lower than the sediments).

Neutron logs measure the absorption of neutrons by hydrogen (typically as H_2O in the SRP), such that porous, water-rich rocks have high neutron

Downloaded from https://pubs.geoscienceworld.org/gsa/geosphere/article-pdf/doi/10.1130/GES01679.1/4663281/ges01679.pdf
by guest

absorption (low backscattered signal), while dense rocks with low porosity and low water contents have low neutron absorption (high backscattered signal to the detector). The absorption of neutrons in water-filled vesicles and fractures contrasts sharply with dense, water-free basalt. Void spaces created by vesicles and fractures are dominantly found in rubbly lava flow tops and flow bases, whereas the massive flow interiors have low porosity. These logs allow us to distinguish individual lava flows and flow units and correlate them with lithologic boundaries found through visual inspection of core.

Paleomagnetic Analyses

More than 1200 subcore samples were obtained over the entire 1912 m length of the drill core for paleomagnetic analysis. Samples were subjected to alternating field (AF) and thermal demagnetization protocols best described by Champion et al. (2011). Prior to sampling, the core was stratigraphically logged and described using the protocols of Davis et al. (1997), and the boundaries between flows and flow units were identified. Depths were measured from markers recorded by the drillers at the time of coring and placed within the core boxes.

Each 2.5 cm subcore was drilled at right angle to the axis of each chosen slug of original drill core to provide material for paleomagnetic analysis and trimmed to 2.2 cm length. Because the Kimama borehole was cored without azimuthal control, no absolute declination data can be obtained from these samples. Only inclination value and remanent magnetic polarity could be obtained using a 2G200 analog-signal cryogenic magnetometer. The accuracy of the inclination data obtained requires the original borehole to be vertical in its orientation. A gyroscopic deviation log of the Kimama borehole was made at 0.3 m intervals, and it reveals deviations from vertical typically less than one degree, verifying the inclination data.

Progressive AF demagnetization was performed on nearly all samples to remove any components of secondary magnetization. Most demagnetization sequences document simple primary magnetizations when plotted on vector component diagrams. A common secondary magnetization called "drill string remanence," oriented vertically downward, is present in many demagnetization sequences, but is easily removed at low AF peak-field values. A few samples, particularly near polarity and sharp inclination value transitions, were thermally demagnetized to better remove low-T opposite polarity overprinting thermal remagnetization.

The primary or characteristic remanent inclinations measured on each individual basalt subcore sample were tabulated over the length of the Kimama borehole. The challenge is to identify the total thickness of each lava flow encountered. Coupled with the stratigraphic log of the drill core, the characteristic inclination and/or polarity value of each successively deeper subcore was compared to those above it. Barring the imposition of a sediment, soil, or zone of oxidation between the subcores, if the characteristic inclinations were in agreement, then the lava flow was deemed thicker. Eventually, the next deeper sample, usually separated by at least a flow unit boundary, was found to have a different characteristic inclination and/or polarity, and the total thickness of the previous flow would be established.

The thickness and number of subcore samples within individual inclination-defined flows varied from 1 to 151 m, and 2 to 100 samples. Mean inclination values for each lava flow group, alpha 95 ($\alpha 95$), and kappa were calculated using an algorithm suggested by McFadden and Reid (1982) (Table 1). Alpha-95 values (standard error measures) are strongly dependent on the number of samples in the population. Thus, small data populations (N = 2 or 3) have large uncertainties, and large populations (N = 100) have very small uncertainties. The kappa values (inverse standard deviation measures) typically range from 200 to 1000 and are not dependent on population size. Characteristic inclination values derived for samples from the deepest paleomagnetic time unit, paleomagnetic time unit 54 (corresponds to flow groups 76–78), did not conform to the demagnetization behavior displayed by shallower samples. In particular, the vector component diagrams were not simply interpretable. Basalt flows at this depth are interbedded with hyaloclastic basalt tephra layers and show aspects of chemical alteration. Thus, physical disruption of the flow sequence from phreatomagmatic syneruptive events is possible. Additionally, although the temperature at T.D. was found to be ~59.3 °C, geothermometers imply temperatures ranging from 125 to 140 °C (Lachmar et al., 2017). Higher bottom-hole temperatures present the possibility of both thermal and chemical partial remagnetization of samples from these depths. Our demagnetization protocol, successful on samples stratigraphically above, requires additional study for these samples. We therefore represent the range of their typical inclination and polarity variation. They do systematically represent reversed polarity, not acquired over the past 780 k.y., and that is the only use we make here of that stratigraphic interval.

The mean remanent inclination values found for the 54 paleomagnetic time units and 78 lava flow groups range from 5° to –40°, but most group mean values vary between ±50° and ±70°, near the expected axial dipole average inclination of 61° for the Kimama borehole location. The mean inclinations and polarity stratigraphic intervals were then compared to the geomagnetic polarity time scale (Gradstein et al., 2012). They match the time sequence of magnetochrons and subchrons in an almost unbroken linear manner.

^{40}Ar-^{39}Ar Age Determinations

Age determinations for six samples from the Kimama drill core were derived from groundmass separates. The groundmass samples were prepared from whole-rock drill-core pieces by crushing and sieving to obtain a 200–300-μm-size fraction and were then acid leached following the procedure described by Koppers et al. (2000). This consisted of 15 min sequential leaching in 1 N HCl, 5 N HCl, 1 N HNO_3, and 5 N HNO_3. Before irradiation, 50–100 mg of material were sorted from the final leached separate to remove fragments of phenocrysts and any remaining alteration minerals. All samples were irradiated

Downloaded from https://pubs.geoscienceworld.org/gsa/geosphere/article-pdf/doi/10.1130/GES01679.1/4663281/ges01679.pdf
by guest

TABLE 1. PALEOMAGNETIC CHARACTERISTICS OF KIMAMA DRILL CORE SUPER GROUPS AND FLOW GROUPS

Chron/subchron	Paleomagnetic age range (Ma)	Paleomagnetic time unit	No. of samples	Polarity and inclination (°)	α95	K	Super group	Flow group	Depth range (m)
BRUNHES	0.72–0.78	1	8	59.6	1.5	1156	**A**	1	0–118.3
		2	61	50.6	0.7	445		2	
		3	3	42.7	11.8	1268		3	
		4	11	37.9	1.7	544		4	
MATUYAMA (a)	0.78–0.99	5	18	–55.7	1.0	774	**B**	5	123.7–183.8
		6	16	–63.2	1.7	317		6	
		7	12	–63.9	1.1	1094		7	
Jaramillo	0.99–1.07	8	18	22.2	0.8	1304	**C**	8	202.3–232.8
MATUYAMA (b)	1.07–1.78	9	65	–61.5	0.7	452	**D**	9	237.4–248.2
			65	–61.5	0.7	452		10	
			65	–61.5	0.7	452		11	
		10	2	–63.0	2.8	837	**E**	12	
		11	15	–64.0	1.8	315	**F**	13	
		12	29	–61.8	0.9	557		14	
			29	–61.8	0.9	557		15	
			29	–61.8	0.9	557		16	
		13	35	–57.0	0.9	500		17	
Olduvai	1.77–1.95	14	7	60.2	2.1	741	**G**	18	425.1–527.4
		15	8	57.2	1.7	857		19	
		16	25	22.0	0.8	798	**H**	20	
			25	22.0	0.8	798		21	
			25	22.0	0.8	798		22	
		17	11	26.9	1.4	768	**I**	23	
		18	14	55.6	1.5	484		24	
			14	55.6	1.5	484		25	
MATUYAMA (c)	1.95–2.43	19	8	–51.7	1.6	935	**J**	26	528.3–708.0
		20	97	–53.9	0.6	338		27	
			97	-53.9	0.6	338		28	
			97	–53.9	0.6	338		29	
			97	–53.9	0.6	338		30	
		21	6	–54.9	0.9	4740		31	
X-Event	2.43	22	11	32.2	2.1	339	**K**	32	708.0–731.8
MATUYAMA (d)	2.43–2.58	23	13	–58.0	2.6	186	**L**	33	732.4–910.9
		24	11	–62.4	1.7	542		34	
		25	38	–44.8	0.9	486		35	
		26	11	-65.3	2.3	299		36	
		27	21	–40.4	1.1	555		37	
		28	20	–54.8	1.9	212		38	
GAUSS (a)	2.58–3.05	29	15	65.2	1.5	465	**M**	39	910.9–934.4
Kaena	3.05–3.12	30	7	–76.6	2.5	516	**N**	40	934.4–950.0
		31	1	–73.3	—	—		41	
		32	1	–76.4	—	—		42	
GAUSS (b)	3.12–3.22	33	10	65.0	2.0	459	**O**	43	950.0–961.5
Mammoth	3.22–3.33	34	35	–59.7	0.9	495	**P**	44	962.0–974.5
			35	–59.7	0.9	495		45	
			35	–59.7	0.9	495		46	
			35	–59.7	0.9	495			
GAUSS (c)	3.33–3.58	35	8	63.1	2.7	331	**Q**	47	974.5–1076.6
		36	23	50.9	1.1	481	**R**	48	
			23	50.9	1.1	481	**S**	49	
			23	50.9	1.1	481	**T**	50	
GILBERT (a)	3.58–ca. 3.9	37	25	–72.0	1.3	357	**U**	51	1077.1–1112.9
		38	25	–72.0	1.3	357	**V**	52	
Unknown excursion	ca. 3.9	39	3	4.7	6.0	4900	**W**	53	1113.3–1115.8
GILBERT (b)	ca. 3.9–4.17	40	10	–69.4	2.3	347	**X**	54	1116.5–1151.0
		41	9	–48.7	4.5	103		55	
		41	9	–48.7	4.5	103		56	
Cochiti	4.17–4.29	42	51	58.2	1.0	288	**Y**	57	1151.9–1234.7
			51	58.2	1.0	288		58	
			51	58.2	1.0	288	**Z**	59	
			51	58.2	1.0	288	**AA**	60	
		43	9	65.8	2.2	418		61	
GILBERT (c)	4.29–4.48	44	2	–59.5	3.4	568	**AB**	62	1236.1–1237.0
Nunivak	4.48–4.62	45	100	58.7	0.7	273	**AC**	63	1239.5–1377.1
			100	58.7	0.7	273		64	
			100	58.7	0.7	273		65	
GILBERT (d)	4.62–4.98	46	10	–42.6	3.1	186	**AD**	66	1379.0–1407.0
		47	12	–57.7	1.9	382		67	
Thvera	4.98–5.23	48	38	67.6	1.1	331	**AE**	68	1411.5–1526.3
		49	35	61.5	1.3	241		69	
		50	6	42.6	4.4	218		70	
GILBERT (e)	5.25–5.89	51	17	-45.0	2.1	200	**AF**	71	1527.0–1729.7
		52	96	–67.2	0.8	217		72	
			96	–67.2	0.8	217		73	
			96	–67.2	0.8	217		74	
C3An (a)	5.89–6.14	53	9	64.2	3.6	162	**AG**	75	1754.1–1767.8
C3an.1	6.14–???	54	—	–40 to –50	—	—	**AH**	76	1768.5–1912.0
			—	–40 to –50	—	—		77	
			—	–40 to –50	—	—		78	

Notes: Paleomagnetic classification, age determination, number of samples, polarity, mean inclination, α95, and kappa (K) calculations, and depth range of Kimama drill core super groups and flow groups. Flow groups were determined using major and trace element geochemical variation (Potter et al., 2018), stratigraphy, and paleomagnetic characteristics. Super groups are classified based upon magnetic chron and geochemical signatures and represent coeval flow groups erupted from unrelated magma reservoirs (Hughes et al., 2002). Paleomagnetic analyses were conducted at the U.S. Geological Survey Volcano Science Center Paleomagnetic Laboratory, Menlo Park, California. Number of samples is total number of sequential specimens, spanning variable depth intervals in the corehole. Polarity, mean inclination (+ normal polarity/– reversed polarity), α95, and kappa (K) are calculated results using the algorithm of MacFadden and Reid (1982).

Downloaded from https://pubs.geoscienceworld.org/gsa/geosphere/article-pdf/doi/10.1130/GES01679.1/4663281/ges01679.pdf
by guest

at the Oregon State University 1 MW TRIGA reactor. Neutron flux was monitored using a Fish Canyon Tuff biotite (FCT-3) with a monitor age of 28.02 ± 0.16 Ma (Renne et al., 1998). Argon extraction and analysis were achieved with a Merchantek 10 W CO_2 laser and a MAP 215-50 mass spectrometer following the methods outlined in Duncan and Hogan (1994) and Duncan et al. (1997). Data reduction utilized ArArCALC v. 2.2 (Koppers, 2002) using decay constants proposed by Steiger and Jäger (1977).

Samples were heated from 400° to 1400 °C (fusion) in seven to eight steps with gas cleanup and Ar-isotopic measurement after each temperature step. Ages were calculated from the isotopic data in a number of standard ways. Total fusion ages incorporate all heating steps in a given incremental heating experiment, essentially equivalent to a conventional K-Ar age determination. Plateau ages, calculated as the weighted mean (by inverse variance) of multiple step ages, are considered reliable if they include three or more contiguous step ages constituting >50% of the total gas released. A statistical parameter, mean square of weighted deviates (MSWD), compares error within step ages with scatter about the mean step age. Ages are considered significant for MSWD values below ~2.5 (depending on the number of heating steps). Isochron ages are calculated from the slopes of linear regressions through the step isotopic compositions ($^{40}Ar/^{36}Ar$ vs. $^{39}Ar/^{36}Ar$) that comprise the plateaus and make no assumption about the initial Ar composition ($^{40}Ar/^{36}Ar$).

Our analyzed samples show petrographic evidence for low-temperature alteration to clays and zeolites. In such cases, the possibility for ^{40}Ar loss and K addition during fluid-rock chemical exchange is significant. Baksi (2007) compared fresh and altered basalts dated by ^{40}Ar-^{39}Ar incremental heating experiments and developed several quantitative measures of levels of alteration at which age data may be compromised. The first is the concentration of ^{36}Ar (atmospheric, corrected for reactor produced ^{36}Ar from Ca), which lies below ~3×10^{-14} mol/g for whole-rock basalts in samples that produced acceptable (crystallization) plateau ages.

Geophysical Data as a Proxy for Drill Core

Slimhole drilling used with neutron and natural gamma-ray logs is a relatively low-cost, time-effective, and accurate means of determining viable geothermal targets. Although drill-core data provide the most reliable and tangible means of characterizing the subsurface, the use of geophysical wireline logs is a reliable proxy for identifying flow boundaries, geochemical transitions, and probable routes for fluid transport in the subsurface (e.g., Kessler et al., 2017). The comparison of logging methods employed to characterize the Kimama drill core provides clear evidence that neutron wireline logs correlate closely to actual basalt flow breaks.

The pronounced fluctuation of neutron and natural gamma-ray measurements closely mirrors the location of massive flow interiors and associated flow boundaries. Increased signal response in both natural gamma-ray and neutron logs correlates to actual sediment interbed locations identified during lithologic logging. Especially at depths of 735 m and 1226 m, spikes and drops in natural gamma-ray and neutron log signals accurately identify the presence of sediment interbeds and flow unit boundaries.

Many basalt flow group breaks within the Kimama drill core are delineated by the presence of sediment in fractures and vesicles. Although not a robust tool for determining avenues of porosity between basalt flows, natural gamma-ray logs highlight geochemical anomalies within the basalt stratigraphy that could indicate changes in magma generation processes and associated volcanism. Furthermore, natural gamma-ray logs provide a valuable resource in determining sample locations for geochemical studies.

RESULTS

Paleomagnetic Stratigraphy and Relative-Age Dating

Fifty-four independent paleomagnetic eruptive episodes were recognized on the basis of alternating magnetic polarity and mean remanent inclination values (Fig. 5 and Table 1); these are further grouped into 34 super groups based upon paleomagnetic chron or subchron designation and 78 flow groups based upon geochemistry. Basalt flow contacts and the interior portions of thick sediment interbeds mark the boundary between magnetic polarity events, which comprise 11 normal polarity intervals and 11 reversed polarity sequences. Thick sediment interbeds are almost entirely absent from the Kimama drill core, limiting the length of volcanic hiatuses to less than tens to hundreds of thousands of years (Champion et al., 2011).

Polarity, ^{40}Ar-^{39}Ar age determinations, and stratigraphic data from the Kimama drill core are consistent with the presence of five paleomagnetic chrons, eight paleomagnetic subchrons, and two excursions. Polarity measurements and depths from basalts in the Kimama drill core are consistent with values determined for the Brunhes normal polarity chron, the Matuyama reversed polarity chron, the Gauss normal polarity chron, the Gilbert reversed polarity chron, and the C3An normal polarity chron. The Jaramillo, Olduvai, Kaena, Mammoth, Cochiti, Nunivak, Thvera, and C3an.1 subchrons are also recognized, as well as the "X" event and an unknown excursion (Table 1) (Champion et al., 2011; Gradstein et al., 2012). Several paleomagnetic boundaries in the Kimama drill core correlate to paleomagnetic boundaries identified in other SRP scientific drill cores at depth, i.e., NPRE, INL-WO-2, and Wendell Regional Aquifer Systems Analysis (Wendell-RASA) (Champion et al., 2002; Morse and McCurry, 2002; Jean et al., 2013).

Polarity measurements from samples taken from the uppermost 118 m of the Kimama drill core are consistent with the Brunhes normal polarity chron. Basalts recovered from ~202–234 m depth and 425–527 m depth exhibit inclination ranges and polarity consistent with the Jaramillo and Olduvai normal polarity subchrons (respectively) within the Matuyama reversed polarity chron (124–911 m depth). Basalts exhibiting inclination ranges and polarity consistent with the Kaena and Mammoth reversed polarity subchrons were

Downloaded from https://pubs.geoscienceworld.org/gsa/geosphere/article-pdf/doi/10.1130/GES01679.1/4663281/ges01679.pdf
by guest

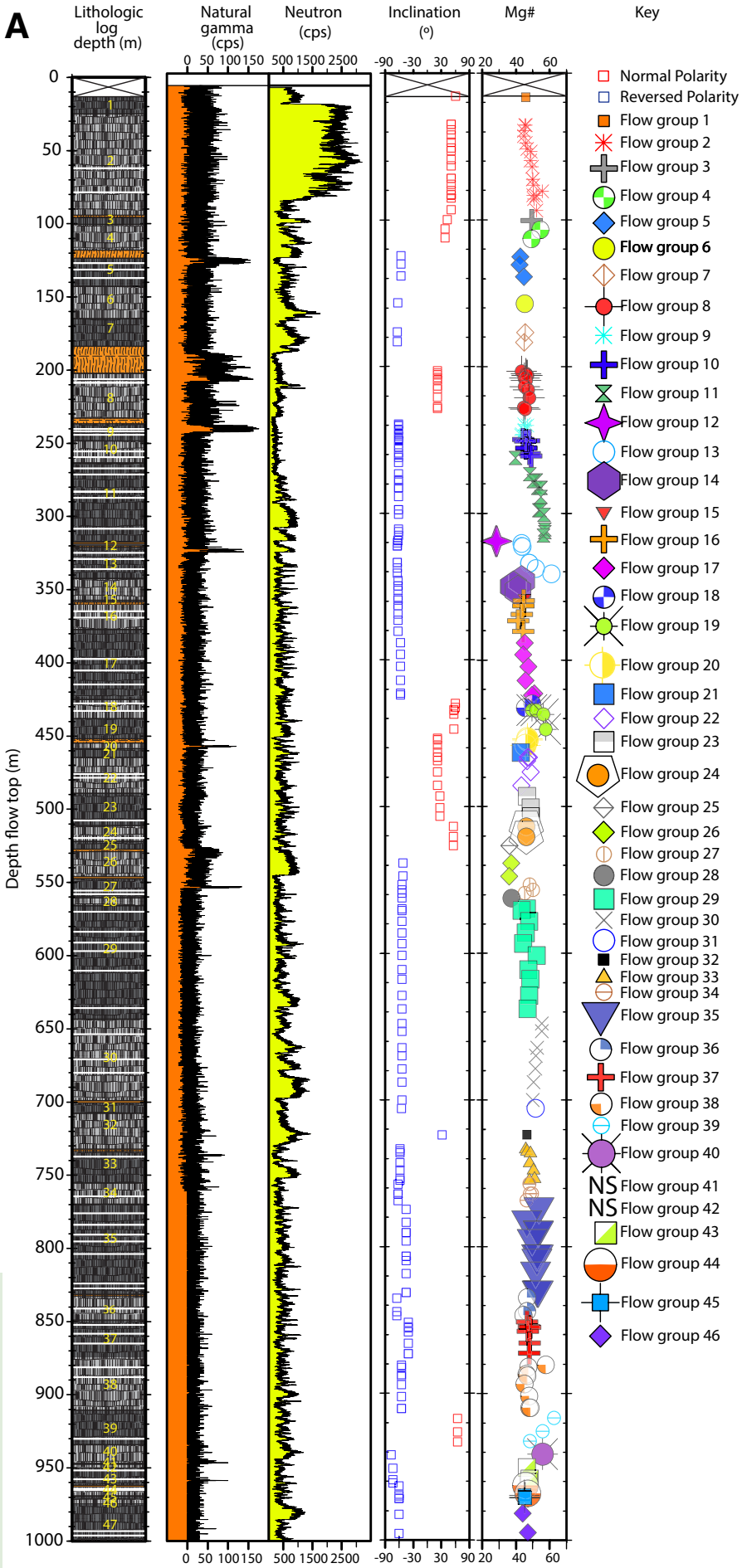

Figure 5. Composite lithologic, natural gamma (cps), neutron (cps), paleomagnetic inclination, geochemistry (as Mg#) logs from the Kimama borehole. All data sets were used to categorize Kimama basalts into 78 flow groups (numbered) and 183 flows, boundaries indicated as white lines, consisting of 1–20 flow units. The 432 flow units are not shown. Four flow groups were not sampled in the drill core and are labeled "NS." Sediments are denoted by symbology and color to represent loess (orange), sandstone (red), sandy silt-siltstone (yellow), and hyaloclastite (purple). Geochemical and paleomagnetic inclination and polarity are represented using the same symbols to illustrate variations by flow group. (A) Composite logs from the surface to 1000 m depth. (B) Composite logs for 1000–1912 m depth. Correlation between the natural gamma ray logs and stratigraphic and geochemical data is apparent at 319 m depth, where an evolved, high K-Fe flow group (flow group 12) is imaged by an abrupt increase in the natural gamma signal. (*Continued on following page.*)

Downloaded from https://pubs.geoscienceworld.org/gsa/geosphere/article-pdf/doi/10.1130/GES01679.1/4663281/ges01679.pdf
by guest

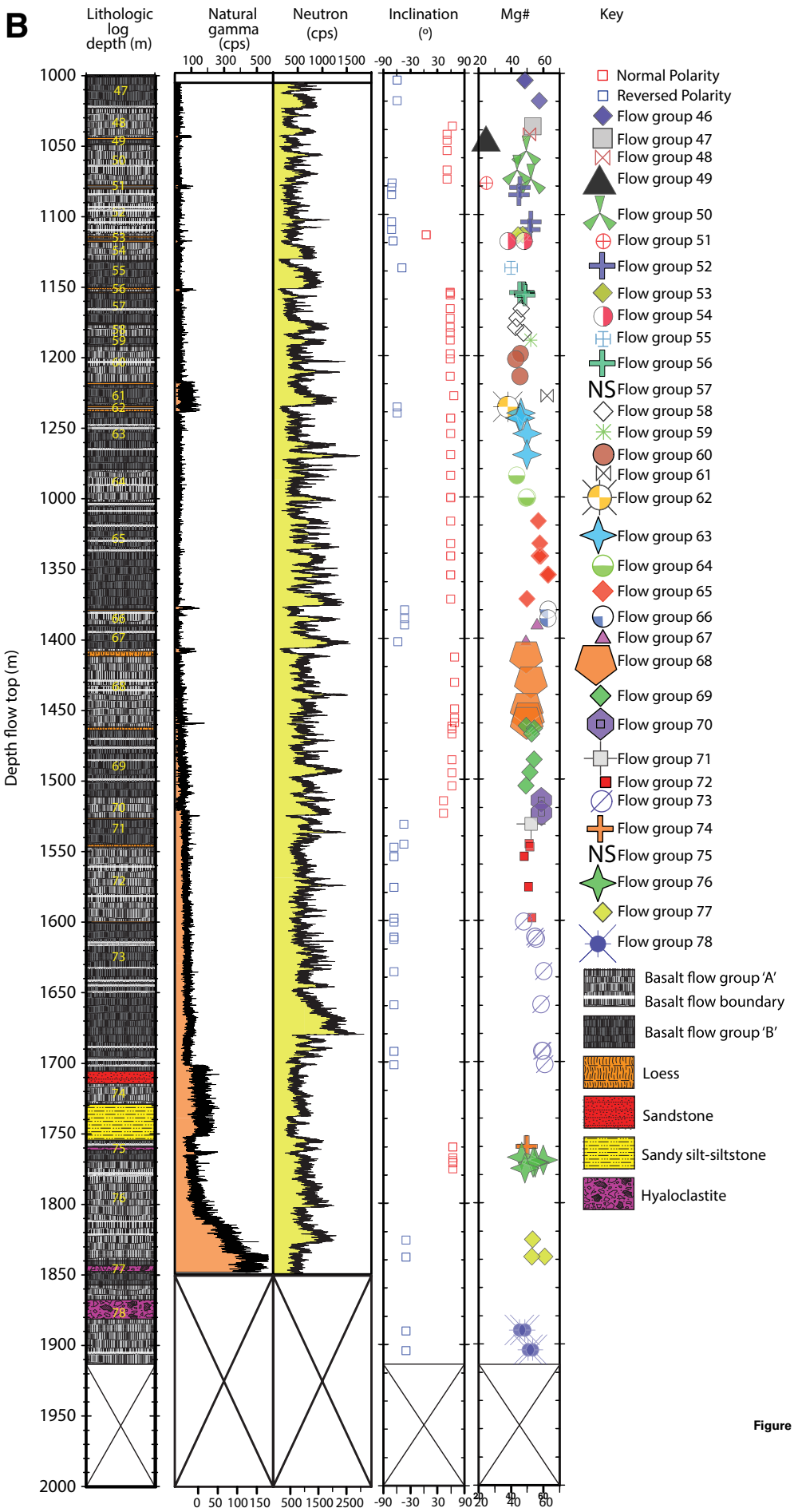

Figure 5 (*continued*).

Research Paper

Downloaded from https://pubs.geoscienceworld.org/gsa/geosphere/article-pdf/doi/10.1130/GES01679.1/4663281/ges01679.pdf
by guest

identified between 934–950 m depth and 962–975 m depth (respectively) within the Gauss normal polarity chron (911–1077 m depth). Polarity and inclination ranges consistent with the Cochiti, Nunivak, and Thvera normal polarity subchrons were identified in basalts between 1113 and 1116 m depth, 1152–1235 m depth, and 1412–1526 m depth (respectively) within the Gilbert reversed polarity chron (1077–1730 m depth). Basalts from 1730 to 1912 m depth (T.D.) exhibit polarity consistent with the C3An normal polarity chron. Normal polarity paleomagnetic inclinations of Kimama flow groups range from 5° to 68°, mean 51°, while reverse-polarity inclinations range from –40° to –77° (mean –59°) with minor variation within flows of each flow group.

^{40}Ar-^{39}Ar Radiometric Dating

Total fusion, plateau, and isochron ages are summarized for all analyzed samples in Table 2. Age spectra and isochron plots are shown in Figure 6. In general, the incremental heating experiments produced clear age plateaus composed of most of the gas released. Although some step ages appear to be influenced by irradiation-induced ^{39}Ar, ^{37}Ar recoil, resulting in old low-temperature step ages in samples KMAB1488 (454 m depth) and KMA4788 (1459 m depth) and young high-temperature step ages in sample KMA3791 (1155 m depth); none of the samples appears to be affected by ^{40}Ar loss.

The six samples from the Kimama drill-core hole provided reliable plateau ages, composed of 86%–100% of the total gas released, ranging from 1.54 to 5.05 Ma (Table 1). The ages generally increase with depth in stratigraphic order. The exception is sample KMA4214 (1284 m depth), which has a weighted plateau age of 4.18 ± 0.58 Ma and is younger than sample KMA3885 (1184 m depth, 4.39 ± 0.30 Ma). In all cases, plateau ages are consistent with isochron ages and show no evidence for significant recoil, or ^{40}Ar loss (Fig. 6). Because the step compositions do not typically show large ^{39}Ar/^{40}Ar variations, the slope regressions of ^{36}Ar/^{40}Ar versus ^{39}Ar/^{40}Ar are not well constrained, and the analytical uncertainties for isochron ages are larger than for corresponding plateau ages. In all cases, however, the plateau and isochron ages are concordant and initial ^{40}Ar/^{36}Ar compositions are indistinguishable from the atmospheric value (295.5) (Nier, 1950).

Thus, we find no evidence for unequilibrated "excess" ^{40}Ar during cooling, and we report the plateau ages as our best estimate of the times of crystallization of these lava flows. ^{36}Ar concentrations, calculated as a quantitative measure of alteration (Baksi, 2007) from the isotopic data (Table 1), are below the suggested cutoff value for whole rocks. Hence, alteration and ^{40}Ar loss have not significantly compromised the measured plateau ages as reliable estimates of the times of crystallization of these lava flows.

Lithostratigraphy and Geochemistry

Lithologic observations and geochemical analyses indicate the presence of 78 flow groups of one to ten flows each, 183 flows of one to 20 flow units each, and 432 flow units (Table 3). Forty-two sediment interbeds are collectively ~107 m thick and make up ~6% of the drill core, ranging in thickness from 0.6 m (loess interbed, 972 m depth) to 24.5 m (fluvial interbed, 1730 m depth). In the upper 1705 m of drill core, loess beds are a combined thickness of 54 feet. Sediments below 1705 m depth are a combined thickness of 53 m and show bedding and grain-size variations consistent with a fluvial origin. The frequency of sediment interbeds gradually increases below 1000 m, with flow groups 65–77 bounded by sedimentary interbeds. Fifty percent of sediments in the Kimama drill core are fluvial and occur within 207 m, between 1705 m and T.D. Thick loess interbeds in the upper 1705 m of the drill core are clearly visible in the natural gamma-ray logs as high gamma-ray spikes (Fig. 5A).

Hyaloclastites (Figs. 4N and 5B) are found in flow groups 75, 77, and 78 at depths of 1757–1761 m, 1843–1848 m, and from 1858 to 1861 m (Table 3). In the Kimama drill core, hyaloclastites are angular basalt breccias bounded by a matrix of sand and basaltic glass fragments, which have been subsequently altered and silicified by hydrothermal fluids.

TABLE 2. ^{40}Ar-^{39}Ar AGE DETERMINATIONS FOR KIMAMA DRILL CORE

Sample	Depth (m)	Total fusion (Ma)	2σ error (Ma)	Plateau age (Ma)	2σ error (Ma)	N	MSWD	Isochron age (Ma)	2σ error (Ma)	MSWD	^{40}Ar/^{36}Ar initial	2σ error	^{36}Ar E-14 (mol/g)
KMA1050	320	1.47	0.23	**1.54**	0.15	8/8	0.29	1.63	0.30	0.25	294.6	2.3	0.185
KMA1488	454	1.78	0.18	**1.62**	0.15	7/8	0.44	2.25	1.34	0.35	288.7	14.7	0.151
KMA3791	1155	3.58	0.20	**3.74**	0.13	6/8	0.39	3.79	0.15	0.18	294.5	1.7	0.127
KMA3885	1184	4.17	0.64	**4.18**	0.58	7/7	0.43	3.97	0.71	0.48	296.5	2.6	0.079
KMA4214	1284	4.40	0.40	**4.39**	0.30	7/7	0.04	4.40	0.31	0.04	295.1	5.6	0.058
KMA4788	1489	5.70	0.93	**5.05**	0.81	6/7	0.23	4.87	1.20	0.27	297.1	8.5	0.063

Notes: ^{40}Ar-^{39}Ar age measurements for six Kimama basalt samples. Ages calculated using biotite monitor FCT-3 (28.02 Ma) and the total decay constant $\lambda = 5.530E^{-10}$/yr. N is the number of heating steps (defining plateau/total); mean square of weighted deviates (MSWD) is an F statistic that compares the variance within step ages with the variance about the plateau age. Preferred (plateau) ages are shown in bold, concordant with isochron ages. Ages were obtained at Oregon State University Argon Geochronology Lab.

Downloaded from https://pubs.geoscienceworld.org/gsa/geosphere/article-pdf/doi/10.1130/GES01679.1/4663281/ges01679.pdf
by guest

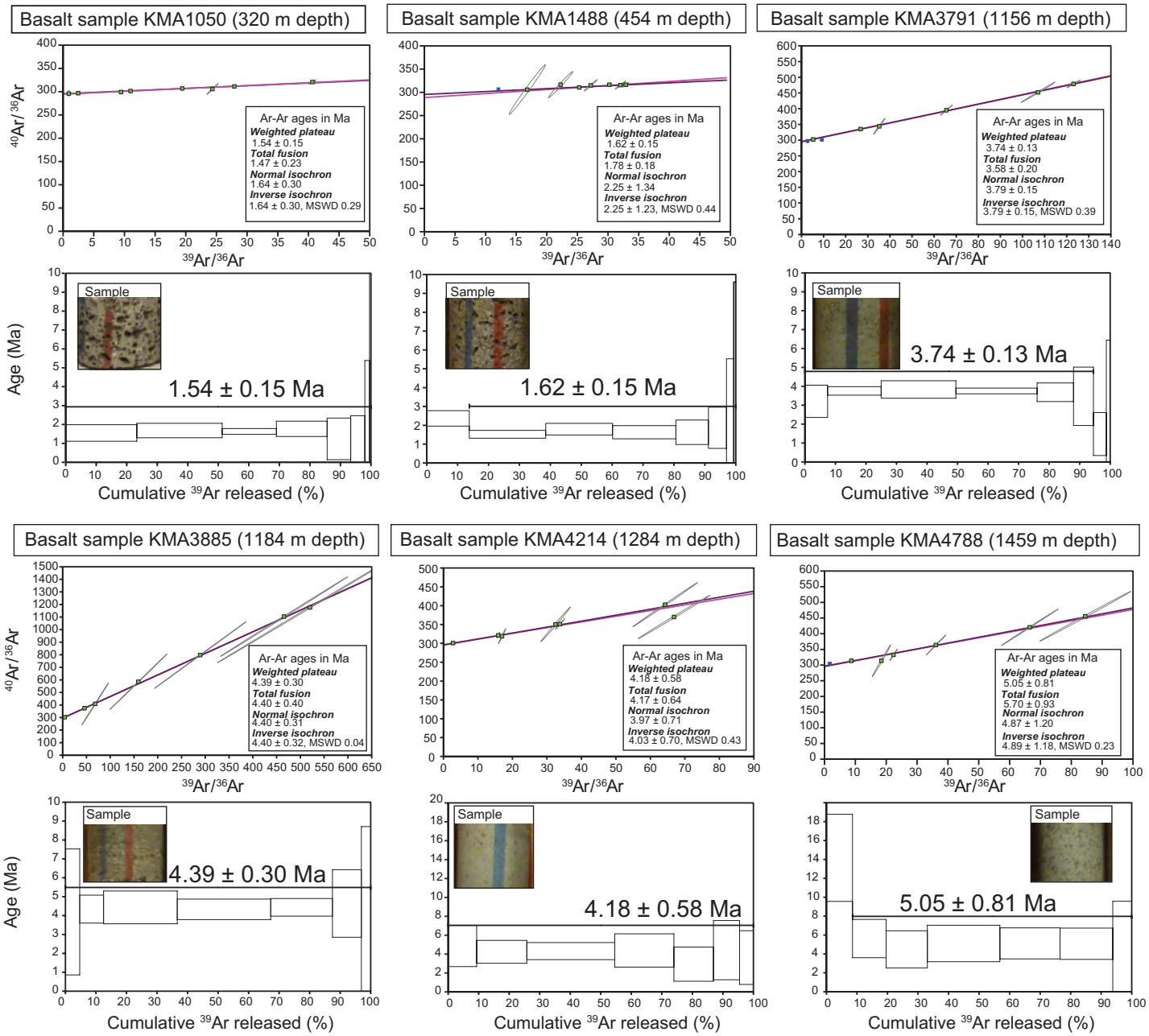

Figure 6. Step age spectra and Ar/Ar isotope correlation diagrams from $^{40}Ar/^{39}Ar$ incremental heating experiments from Kimama basalt samples. Analyses were performed at Oregon State University. The upper figures are isotope correlation diagrams where the intercept of the regression represents the initial $^{40}Ar/^{36}Ar$ ratio. The lower figures show the step age spectrum; the thickness of the bar indicates the ±1σ external error, and the horizontal lines adjacent to the plateau age indicate the steps used to calculate the plateau age. The filled green squares were used in a weighted linear regression to calculate an isochron age. MSWD—mean square of weighted deviates.

Downloaded from https://pubs.geoscienceworld.org/gsa/geosphere/article-pdf/doi/10.1130/GES01679.1/4663281/ges01679.pdf
by guest

TABLE 3. LITHOSTRATIGRAPHY AND BASALT CLASSIFICATION OF THE KIMAMA DRILL CORE

Super group	Flow group	Composition type	No. of flows	No. of flow units	Start depth (m)	End depth (m)	Super group thickness (m)	Flow group thickness (m)	Mean flow thickness (m)	Mean flow unit thickness (m)	Basal sediment thickness (m)
A	1	SROT	1	1	13.4	25.2	104.6	11.7	—	—	—
	2	SROT	3	16	25.2	95.8		70.6	23.5	4.41	0.210
	3	SROT	1	2	96.0	100.6		4.57	—	2.29	—
	4	SROT	1	2	100.6	118.3		17.7	—	8.85	5.49
B	5	SROT	4	10	123.8	142.9	60.1	19.2	4.79	1.92	—
	6	SROT	1	3	142.9	164.8		21.9	—	7.31	—
	7	SROT	1	3	164.8	183.8		19.0	9.49	6.33	18.9
C	8*	SROT	2/3	6/6	202.3/202.3	232.8/232.4	30.5/30.1	30.5/30.1	15.1/10.0	5.02/5.02	4.60/4.39
D	9*	SROT	3/2	6/7	237.4/236.8	248.2/248.5	80.3/80.4	10.8/11.7	3.60/5.86	1.80/1.67	—
	10*	SROT	3/2	6/3	248.2/248.5	264/259.6		15.8/11.1	5.25/5.57	2.63/3.71	—
	11*	SROT	5/5	13/12	264/259.6	317.7/317.2		53.7/57.6	10.7/11.52	4.13/4.80	1.2/0.5
E	12*	High K-Fe	1/1	1/1	318.9/317.7	319.2/318.9	0.274/1.19	0.274/1.19	—	—	0.55/0.8
F	13*	SROT	1/3	4/6	319.7/319.7	329.2/342.5	91.9/105.3	9.44/22.8	—/7.61	4.71/3.80	N/A/—
	14	Fe-Ti	1	7	342.5	357.4		14.9	—	2.13	—
	15	SROT	1	1	357.4	358.7		1.25	—	—	0.152
	16	SROT	3	8	358.8	377.2		18.4	6.13	2.30	—
	17	SROT	4	18	377.2	425.1		47.9	12.0	2.66	—
G	18	SROT	2	5	425.1	432.9	26.5	7.77	3.90	1.56	—
	19	SROT	2	4	432.9	451.7		18.8	9.39	4.69	1.49
H	20	SROT	1	2	453.2	458.7	36.0	5.5	—	2.7	—
	21	Fe-Ti	1	1	458.7	464.7		6.0	—	—	—
	22	SROT	4	9	464.7	489.2		24.5	5.16	2.72	—
I	23	SROT	2	8	482.2	511.3	45.2	29.1	11.1	2.76	—
	24	SROT	2	5	511.3	522.0		10.7	5.36	2.15	—
	25	Fe-Ti	1	1	522.0	527.4		5.36	—	—	0.945
J	26	Fe-Ti	1	2	528.3	547.8	178.9	19.5	—	9.75	0.549
	27	SROT	3	7	548.4	560.7		12.3	3.72	1.59	—
	28	Fe-Ti	1	2	560.7	566.0		5.30	—	2.67	—
	29	SROT (low K)	7	23	566.0	643.5		77.5	11.1	3.37	—
	30	SROT	4	7	643.5	700.6		57.1	14.3	8.16	0.122
	31	SROT	1	1	700.8	708.0		7.19	—	—	—
K	32	SROT	1	1	708.0	731.8	23.8	23.8	—	—	0.640
L	33	SROT	2	6	732.4	755.6	178.1	23.2	11.5	3.82	0.244
	34	SROT	2	5	755.6	770.1		14.5	7.27	2.91	—
	35	SROT	8	21	770.1	831.4		61.2	7.66	3.6	0.366
	36	SROT	2	4	831.7	849.1		17.4	8.7	4.35	—
	37	SROT	4	8	849.1	874.3		25.1	11.7	2.44	—
	38	SROT	3	13	874.3	910.9		36.6	9.15	2.82	—
M	39	SROT	2	6	910.9	934.4	23.5	23.5	11.8	3.93	—
N	40	SROT	1	1	934.4	947.2	15.6	12.8	—	—	—
	41	Not sampled	—	—	947.2	948.5		1.25	—	—	—
	42	Not sampled	—	—	948.5	950.0		1.55	—	—	—
O	43	SROT	3	6	950.0	961.5	11.5	11.5	3.83	1.92	0.518
P	44	SROT	3	4	962.0	969.1	12.2	7.01	2.34	1.75	0.183
	45	SROT (low K)	1	2	969.2	971.6		2.35	—	1.17	0.061
	46	SROT	1	2	971.6	974.5		2.84	—	1.42	—
Q	47	SROT	3	7	974.5	1022.1	47.6	47.6	15.9	6.80	—
R	48	SROT (low K)	1	2	1022.1	1044.1	22.1	22.1	—	8.30	0.914
S	49	High K-Fe	1	1	1045.0	1048.8	3.8	3.75	—	—	—
T	50	SROT (low K)	2	3	1048.8	1076.6	27.8	27.8	13.9	9.27	0.549
U	51	High K-Fe	1	1	1077.1	1078.5	1.40	1.40	—	—	0.792
V	52	SROT	6	10	1079.3	1112.9	33.6	33.6	5.60	4.08	0.335
W	53	SROT (low K)	1	1	1113.3	1115.8	2.56	2.56	—	—	0.701
X	54	Fe-Ti	1	2	1116.5	1131.0	34.8	14.4	—	7.22	—
	55	Fe-Ti	1	1	1131.0	1151.0		20.0	—	—	0.914
	56	Not sampled	—	—	1151.9	1152.2		0.300	—	—	0.244
Y	57	SROT (low K)	2	8	1152.4	1175.1	32.3	22.7	11.3	2.83	0.274
	58	SROT	1	2	1175.4	1185.0		9.60	—	4.80	—
Z	59	Evolved	1	1	1185.0	1191.5	6.49	6.49	—	—	—
AA	60	SROT (low K)	2	5	1191.5	1217.1	43.0	25.6	16.2	5.13	0.183
	61	SROT	1	1	1217.3	1234.7		17.3	—	—	1.46
AB	62	SROT (low K)	1	1	1236.1	1237.0	0.880	0.880	—	—	2.44
AC	63	SROT (low K)	4	10	1239.5	1278.8	137.6	39.3	9.85	3.94	—
	64	SROT	3	8	1278.8	1303.6		24.8	8.26	3.10	—
	65	SROT (low K)	5	15	1303.6	1377.1		73.5	14.7	4.90	1.86
AD	66	SROT (low K)	2	2	1379.0	1389.0	27.9	10.0	4.98	4.98	0.152
	67	SROT (low K)	2	3	1389.1	1407.0		17.9	8.93	5.96	4.51
AE	68	SROT (low K)	4	10	1411.5	1460.4	113.8	48.8	12.2	4.88	0.914
	69	SROT (low K)	6	9	1461.3	1510.9		49.6	8.14	5.43	0.762
	70	SROT	1	2	1510.9	1526.3		15.4	—	7.68	0.701
AF	71	SROT (low K)	1	2	1527.0	1545.9	193.4	19.0	—	9.48	0.396
	72	SROT (low K)	3	14	1546.3	1599.5		53.2	16.5	3.54	0.091
	73	SROT (low K)	10	20	1599.6	1705.3		105.7	14.9	3.35	8.84
	74	Not sampled	—	—	1714.1	1729.7		15.6	—	—	24.5
AG	75	SROT (low K)	3	4	1754.1	1767.8	13.7	13.7	8.13	3.42	0.701
AE	76	SROT (low K)	5	11	1768.5	1832.8	124.1	64.3	13.1	5.84	7.80
	77	SROT (low K)	1	2	1840.6	1845.3		4.75	—	1.60	11.6
	78	SROT (low K)	1	5	1856.9	1912		55.1	—	9.63	—

Note: Super group, flow group, flow, flow unit, and sediment stratigraphy of Kimama drill cores 1A and sidetrack 1B as determined from major and trace element geochemistry (Potter et al., 2018), core stratigraphy, and paleomagnetic characteristics. Thicknesses for super groups, flow groups, and average thicknesses for flows and flow units, are shown for drill cores 1A, 1B, and, where overlap exists, both drill cores (1A/1B). Flow groups with an asterisk were sampled by both boreholes 1A and 1B. Flow groups where overlap occurs (flow groups 8–13) are noted by an asterisk. "Basal sediment" (sed.) thickness denotes the thickness of sediment interbeds beneath flow groups. Four different compositional (Comp.) types were recognized on the basis of major-element geochemistry (Potter et al., 2018) and form the basis for defining flow groups: SROT (Snake River Plain olivine tholeiite), high K-Fe, Fe-Ti (high Fe and Ti), Low K, and evolved (high K, Ti, Fe, and low Mg). Flow groups for which no sample was collected are denoted as "not sampled". Please see Supplemental Files (text footnote 1) for complete stratigraphic descriptions.

Downloaded from https://pubs.geoscienceworld.org/gsa/geosphere/article-pdf/doi/10.1130/GES01679.1/4663281/ges01679.pdf
by guest

Flow Groups and Super Groups

Flows and flow units recognized in the Kimama drill core are assembled into flow groups based on their geochemistry, magnetic polarity, and stratigraphic relationships. Flow groups range in thickness from 0.3 m (flow group 12) to 106 m (flow group 73), with an average thickness of 23 m. Four flow groups were not sampled for geochemistry but are identified through paleomagnetic polarity and inclination observations. Boundaries for flow groups 73–78 in the lower ~200 m of core are less certain due to heavy alteration and the presence of brecciated hyaloclastite. The total thickness of basalt in the Kimama drill core is 1805 m, or 94% of the total drill core.

Cycles of increasing and decreasing major- and minor-element concentrations are used to distinguish flow groups, and these group boundaries correlate to lithologic and paleomagnetic divisions. Two cyclical variations are apparent: progressive upsection enrichment in incompatible elements and K_2O. TiO_2 is interpreted to signify fractional crystallization in a magma chamber, while progressive upsection depletion in the same components, coincident with enrichment in compatible elements and MgO, is interpreted to signify magma recharge. A return to baseline Snake River Plain olivine tholeiite (SROT) compositions (0.5–0.8 wt% K_2O, 7–7.5 wt% MgO) signals the beginning of a new geochemical cycle and the eruption of an unrelated batch of magma (i.e., flow group) (Potter et al., 2018). Trace-element concentrations generally mirror trends observed in correlative major-element concentrations. For example, rare-earth elements (REEs), Zr, Nb, and Y demonstrate a positive correlation to FeO*, TiO_2, and P_2O_5; Ba and Rb demonstrate a positive correlation to K_2O; and Ni and Cr correlate positively to MgO. Sharp changes in trace-element concentrations denote a new eruptive episode and flow group.

Upsection geochemical trends within flow groups are thought to represent varying degrees of differentiation in the mafic mid-crustal sill complex, a 10-km-thick network of sill-like plutons and magma chambers located 10–20 km below the surface (Shervais et al., 2006; Potter et al., 2018). Ratios of Ti/K, La/Lu, and Zr/Nb, as well as K_2O, TiO_2, MgO, and total Fe as FeO* wt% plotted against depth were used by Potter et al. (2018) to distinguish cycles of magma recharge, fractional crystallization, or the assimilation of partially crystallized magma in the mafic sill complex (Fig. 2). Ratios of Ti/K and La/Lu are essentially constant during crystal fractionation but vary in magmas formed by different percentages of partial melting or with different source compositions. Tholeiitic basalts from separate magma batches are thus characterized by different minor- and trace-element ratios, which are unique to each flow group. In particular, flow groups display progressive upsection increases in La/Lu, K_2O, and P_2O_5 with decreasing MgO, consistent with progressive assimilation in the mafic mid-crustal sill complex (Potter et al., 2018). On the basis of geochemical analyses and paleomagnetic inclination, interfingering lava flows, which were recognized in the Wendell Regional Aquifer Systems Analysis (RASA) drill core in the ESRP (e.g., Jean et al., 2013), were not recognized in the Kimama drill core.

We have distinguished 78 flow groups, ranging in thickness from 0.3 to 106 m thickness, based upon these criteria and discussed in Potter et al. (2018) (Fig. 5) (Table 3; see also Supplemental Files[1]). Forty-two flow groups, over 90% of Kimama drill core basalts, are defined as SROT based upon compositional trends including 5.00–11.0 wt% MgO, 11.0–15.8 wt% FeO*, 0.15–0.92 wt% K_2O, and 1.2–3.6 wt% TiO_2. SROT flows are recognized in wireline logs as areas of greater neutron signal response than sediment or sediment-coated rubble stratigraphic intervals. Twenty-one SROT flow groups are further divided into low-K_2O endmembers on the basis of K_2O compositional ranges of 0.120–0.403 wt%. These are interpreted to represent secondary alteration (and K_2O loss) of SROT flows below 1200 m depth in the drill core; low K_2O lavas are also correlated to high loss on ignition (LOI) wt%. Seven high–Fe-Ti flow groups have >15 wt% FeO* and >3.6 wt% TiO_2 and represent varying degrees of recharge, fractional crystallization, and assimilation processes acting upon parent SROT magmas. Four flow groups are compositionally unique and are best classified as "Craters of the Moon"–type lavas, characterized by evolved major-element signatures. Flow group 59 has anomalously high SiO_2 and K_2O (53 wt% and 1.6 wt%, respectively) and moderate MgO (6.2 wt%). Three flow groups, 12, 49, and 51, are high–K_2O-FeO* lavas with K_2O >0.65 wt% and FeO* >17.5 wt%. High–K-Fe flow groups, which were initially recognized based on their relatively high gamma signal response, are thought to be geochemically unrelated to SROT and high–Fe-Ti lavas (Potter et al., 2018). Evolved and high–K-Fe flow groups (flow groups 12, 49, 51, and 59) are much thinner than SROT, Fe-Ti, and low-K flow groups and make up less than 1% of the basalt drill core.

At two depth intervals, increased natural gamma-ray signal response is observed without a corresponding K-rich sediment package. Geochemical analyses of samples from 319 m and 1078 m depth (flow groups 12 and 47) demonstrate high K_2O and high FeO* (1.78–1.84 wt% and 17.6–18.4 wt%, respectively) relative to the olivine tholeiite composition of the Kimama olivine tholeiite basalts (0.25–1.00 K_2O wt%; 13.0–17.0 wt% Fe_2O_3) observed in the majority of the drill core (Potter et al., 2018). Elevated K_2O and FeO* compositions in flow groups 12 and 51 are similar to those observed at Craters of the Moon National Monument and Preserve, ~69 km to the northeast (Leeman, 1982; Putirka et al., 2009; Potter et al., 2018).

Basalt super groups are collections of coeval flow groups erupted from unrelated magma reservoirs (Hughes et al., 2002). Although flow groups within a super group share the same magnetic polarity, they are geochemically different. The 34 super groups identified in the Kimama drill core range in thickness from 0.3 m (super group E, high K-Fe) to 193.4 m (super group AF, low-K) (Table 3). Variability in mean paleomagnetic inclination data within a super group suggests an elapsed duration of centuries to tens of thousands of years (Champion et al., 1988; Champion, et al., 2011).

Flows and Flow Units

Flows are recognized based on differences in magnetic polarity, remanent magnetic inclination, and lithostratigraphy. Based upon stratigraphic observations, almost all of the lava flows identified in the Kimama drill core

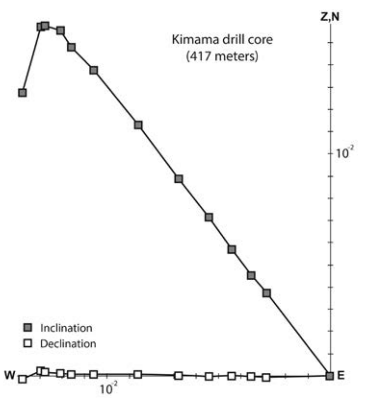

Supplemental Figure 1: Vector component diagram for alternating-field (AF) demagnetization of basalt sample from 417 meters depth in Kimama drill core.

[1]Supplemental Files. Detailed lithologic log of the Kimama drill core. Please visit https://doi.org/10.1130/GES01679.S1 or access the full-text article on www.gsapubs.org to view the Supplemental Files.

Downloaded from https://pubs.geoscienceworld.org/gsa/geosphere/article-pdf/doi/10.1130/GES01679.1/4663281/ges01679.pdf
by guest

are compound lava flows comprising two or more flow units. There are a few simple flows composed of a single flow unit, but these are generally thin sheets that are geochemically and lithologically distinct from flows above and below, classifying them as flow groups (flow groups 12, 49, 51, and 59). Flow units are characterized by mappable upper and lower contacts, e.g., glassy, oxidized, and ropey surfaces, overlying vesicular zones that grade into massive interiors (Fig. 3); as noted above, this lithologic transition is represented in the neutron logs as a sawtooth pattern of signal intensity (Fig. 5). Flow units within a compound lava flow are commonly in direct contact with other flow units in that flow.

Within a basalt flow, flow units share the same general chemistry but are distinguished by lithologic facies. Flow units range in thickness from 0.3 m to 30 m (most 0.3–5 m thick; 4 m average). Using lithologic observations, petrography, and geochemical and paleomagnetic stratigraphy, we grouped flow units into 183 lava flows, 0.3 m to 48 m thick (most 1–10 m thick; 10 m average). Flows and flow units are summarized in Table 3 and reviewed in detail in the Supplemental Files [footnote 1]. Massive basalt flows are commonly overlain by multiple pahoehoe flow units and periodically show evidence of sediment-coated weathering surfaces along cooling boundaries.

DISCUSSION

Volcanic Stratigraphy

The Kimama drill core contains 432 flow units that are grouped into 183 lava flows, 78 flow groups, and 34 super groups (Table 3). Flows contain 1–20 flow units that are grouped by lithologic relationships, and each flow group is made up of one to ten flows that have the same paleomagnetic inclination and similar major- and trace-element composition. Most flow groups are compositionally similar to typical SROT basalts (Potter et al., 2018). Flow groups may be bounded by sediment interbeds, but sediment interbeds are never present within flow groups. Flow groups have an average thickness of 23 m but range between 0.3 m to 106 m thick (flow groups 12 and 73, respectively) and are estimated to have erupted over durations of decades to ~200 years.

Stratigraphic correlation between the Kimama drill cores 1A (13 m to 329 m depth) and 1B (202 m to 1912 m depth) is possible over 127 m (Table 3). This overlap presents a rare opportunity to examine the stratigraphic continuity of basalt flows over a distance of ~7 m from borehole 1A to borehole 1B based upon deviation logs (Twining and Bartholomay, 2011). Flow groups 8 through 13 are recognized in both sections of drill core using stratigraphic characteristics, paleomagnetic inclination, and general geochemistry. The thickness and stratigraphic depth of boundaries are well preserved in flow groups 8 and 9; however, variations as much as 13 m (flow group 13) exist between flow groups sampled by both drill cores. Thickness variations between flows and flow units are generally much smaller: the difference between average flow unit thicknesses between drill cores 1A and 1B ranges from 0 to 1 m, while the difference between average flow thicknesses is slightly larger (0.32–5 m thick) (Table 3).

The representation of flows and flow units also varies between the two boreholes, with the exception of flow group 12. Although its thickness varies by almost a meter between drill cores 1A and 1B, flow group 12 shows no variation in the number of flows or flow units. However, the number of flows and flow units represented in flow groups 8–11 and 13 changes from drill core 1A to 1B (Table 3). The variance between the number of flows and flow units per flow group is generally small, with most flow groups in drill core 1A having a difference of one or two flow units and/or flows from flow groups represented in drill core 1B. We interpret the discrepancy in thickness and the number of flows and flow units to either reflect an incomplete recovery of the flow group in drill core, a missed flow contact, or spatial variations in flow morphology and/or topography across ~7 m.

Sediment interbeds in the two drill cores are largely correlative in both depth of initial occurrence and thickness. In both drill cores, flow group 8 overlies a 14–15-m-thick loess package at 232.8 m (1A) and 232.4 m (1B) depth. Flow groups 11 and 12 contact basal sediment interbeds at 317.7 m (1A) and 317.2 m (1B) and 319.2 m (1A) and 318.9 (m) depths; sediment thicknesses beneath flow groups 11 and 12 are 1.2–0.5 m and 0.6–0.8 m, respectively (Table 3). However, sediment preservation isn't continuous through the drill core. A loess deposit is present beneath flow group 13 in drill core 1A but is absent in drill core 1B between flow groups 13 and 14. This may support the presence of topographic variations and discontinuous sediment accumulation in the immediate vicinity of the Kimama borehole.

Hyaloclastite and the presence of bedding and grain size consistent with fluvial sources indicate periodic phreatomagmatic eruptions. Paleotopographic reconstructions using detrital zircons recovered from fluvial sediments on the surface and in drill core indicate that rivers flowed into the SRP from the north and south immediately following subsidence in the wake of Yellowstone hotspot volcanism (Pierce and Morgan, 1992; Beranek et al., 2006; Hodges et al., 2009). These observations are consistent with the interpretation that the Kimama drill site was situated at a topographic low during which sediments and basalts from 1700 to 1912 m depth accumulated.

The total thickness of the basalt veneer along the CSRP may be estimated by combining the Kimama drill core and the nearby Kimberly drill core into a single record of volcanism. At 55 km to the southwest, the Kimberly drill-core samples basalt lava flows and underlying rhyolite ash flows and provides a record of the basalt-rhyolite contact that is missing in the Kimama drill core. The first 110 m of the Kimberly drill core penetrates much younger Hansen Butte basalt (2.0 Ma; not cored), followed by a ~129 m section of 6.37 ± 0.44 Ma Shoshone Falls Rhyolite (lower 24 m cored). Below the Shoshone Falls Rhyolite are two sections of intercalated basalt and sediment, from 239 m to ~420 m depth; these sections resemble the lowermost section of the Kimama drill core and are older than the Shoshone Falls Rhyolite. The remainder of the drill core samples extremely thick, welded rhyolite ash flows to a total depth of 1958 m depth (Knott et al., 2016). Age data and stratigraphic models

Downloaded from https://pubs.geoscienceworld.org/gsa/geosphere/article-pdf/doi/10.1130/GES01679.1/4663281/ges01679.pdf
by guest

show that basalts and sediments below the Shoshone Falls Rhyolite (from 239 to 420 m) in the Kimberly drill core are slightly older (≥6.37 Ma) than basalts recovered at the base of the Kimama drill core (Shervais et al., 2014; Knott et al., 2016). If we add this 181 m of basalt + sediment in the Kimberly drill core to the 1912 m section penetrated by the Kimama borehole, we can estimate a thickness of 2093 m for Pliocene through Quaternary basalts in the CSRP.

Age and Accumulation Rate

Accumulation rates for basalt volcanism in the ESRP are estimated from standard linear regressions of ages and depths from composite stratigraphic sections of drill core and surface samples recovered from drill-core holes and outcrops throughout the INL (e.g., Anderson and Liszewski, 1997; Anderson et al., 1997). They are also estimated within single drill core stratigraphic successions taken within the INL reservation (Champion et al., 1988; Champion et al., 2002). Paleomagnetic inclination and polarity and K-Ar ages of stratigraphic intervals were determined for basalts deposited during eruptive periods ranging from 200 to 700 ka during the past 1.8 m.y. Rates ranging from 160 m/m.y. to 670 m/m.y. averaging 360 m/m.y. are estimated for areas within the INL (Champion et al., 2002).

Depth intervals of alternating magnetic polarity and subordinate intervals of similar mean remanent inclination values can be organized into 54 paleomagnetic time units, or 34 super groups, ending during the Brunhes normal polarity epoch and beginning within the C3An normal polarity epoch. The median and range of remanent intensity and magnetic susceptibility values remain remarkably constant over the length of the drill core. Density determinations made from the samples are also uniform in their range of values, despite significant alteration evident in the deeper parts of the drill core where temperatures are elevated.

^{40}Ar-^{39}Ar incremental heating determinations for six samples yield plateau ages that generally increase monotonically with depth, with the deepest sample at 1459 m yielding an age of 5.05 ± 0.81 Ma (Fig. 6). Isochron, inverse isochron, and total fusion ages support the plateau age interpretations. The age progression determined from the depths of identified time boundaries in the geomagnetic polarity time scale merges well with the radiometric dates and equally contributes to the age versus depth relationship among the lava flows.

In the bottom 200 m of drill core, basalt flows are interbedded with fluvial sand and hyaloclastite, an indication that lava flows interacted with surface water and sediment. Detrital zircons derived from a juvenile magmatic source were recovered from two fluvial interbeds at depths of 1749 and 1844 m and were dated using laser ablation–inductively coupled plasma mass spectrometry (LA-ICPMS) U-Pb geochronology at the Arizona LaserChron Center. The youngest volcanic zircons in each interbed are interpreted to represent (within analytical uncertainty) the depositional age of the material. The youngest volcanic zircons in the upper fluvial succession (1707–1748 m depth) have ages of 5.8 ± 0.1 Ma, while those in the lower fluvial section (1842–1844 m depth) yield dates of 6.2 ± 0.1 Ma (Potter, 2014).

We calculate an accumulation rate for the Kimama section based upon (1) an age of 475 ± 38 ka (Kuntz et al., 2018) for the surface flow recovered in the Kimama drill core and erupted from Adelaide Butte (Fig. 1); (2) five ^{39}Ar/^{40}Ar ages; (3) 20 geomagnetic polarity time scale age boundaries; and (4) two U-Pb ages from juvenile detrital zircons sampled near the bottom of the drill core (Potter, 2014). A graph of the relationship between the ages of lava flows and their depths in the Kimama drill core documents a linear accumulation rate through time of ~320 m/m.y. (Fig. 7). We project an age of 6.3 Ma for the oldest basalts (or 5.8 m.y. elapsed time).

The 1912-m-thick sequence of basalt lava flows in the Kimama drill core yields ^{39}Ar/^{40}Ar ages that range from ca. 1.54 Ma to ca. 5.05 Ma and paleomagnetic ages that range from 0.48 Ma to 6.14 Ma. A linear regression model fit to age data demonstrates a uniform eruption rate of ~13 flow groups/m.y. and ~30 flows/m.y. in the vicinity of the Kimama borehole. The average volcanic output, projected from ^{40}Ar/^{39}Ar and paleomagnetic ages, was one super group erupted every ~175,735 years, one flow group erupted every ~76,603 years, one flow erupted every ~32,650 years, and one flow unit erupted every ~13,831 years. Sediments were deposited, on average, every ~142,262 years. It is impossible to determine the duration of volcanic hiatuses using the accumulation rate; however, sediment interbeds greater than 24 m thickness may represent over 76,563 years of deposition (and volcanic hiatus) in the vicinity of the Kimama borehole, while the smallest Kimama sediment interbed (0.06 m) may have been deposited over 187 years.

Projections of super group, flow group, flow, flow unit, and sediment accumulation are highly localized because multiple eruptive episodes could have occurred simultaneously without the accumulation of lava flows at the Kimama drill site. Drill core is an imperfect record of volcanism and only preserves a fraction of vent output over a given time period, likely less than 10%–20% of the total volcanic output from vents occurring over a given time period. Therefore, rather than new flow group eruptions occurring every 77,000 years, new flow groups are more likely to erupt every 7600–15,000 years, roughly equivalent to the eruptive output of vents at Craters of the Moon National Monument and Preserve (Kuntz et al., 1986, 2007). Accumulation rates calculated for other boreholes show large variation across the SRP (Anderson and Liszewski, 1997; Anderson et al., 1997; Champion et al., 2002). The accumulation rate calculated for the Kimama borehole (320 m/m.y.) is similar to the average rate calculated for INL boreholes in the ESRP (360 m/m.y.) (Champion et al., 2002).

The accumulation rate calculation for Kimama drill-core basalts can inform the drainage and/or topographic evolution of the Kimama borehole site. Hyaloclastite and fluvial sediments between 1705 m and 1870 m depth indicate that the Kimama borehole site was lower than the surrounding topography. If we apply the accumulation rate and age model to this interval, we can infer that the period between 5.6 and 6.2 Ma was marked by the frequent interaction of lava flows with rivers and lakes in the vicinity of the Kimama borehole site. After 5.6 Ma, multiple, thick packages of fluvial sediment are replaced with relatively rare, <1 m beds of loess, indicating that either the Kimama borehole site was cut off from fluvial sources by other flows, or that the greater

Downloaded from https://pubs.geoscienceworld.org/gsa/geosphere/article-pdf/doi/10.1130/GES01679.1/4663281/ges01679.pdf
by guest

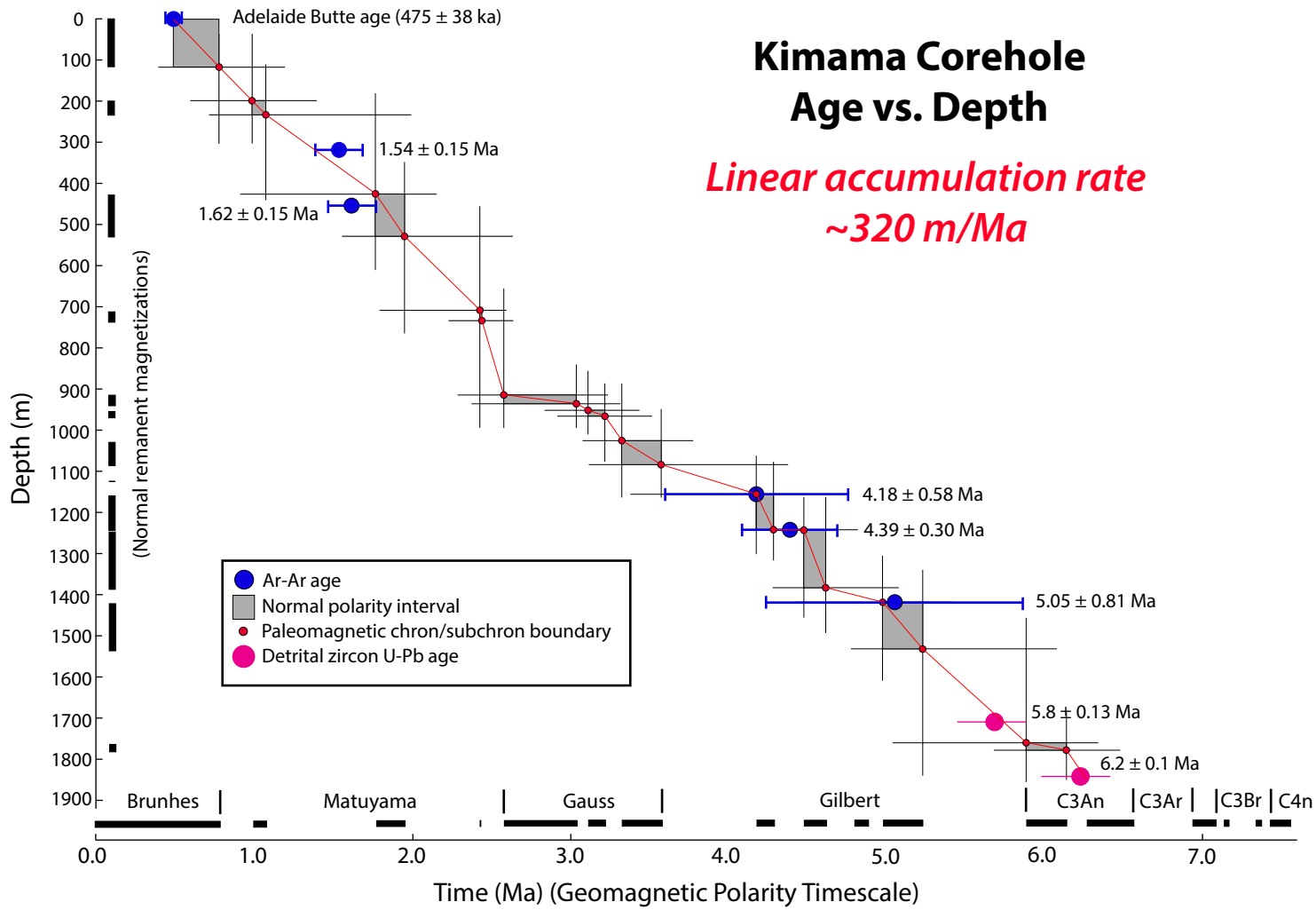

Figure 7. Accumulation rate estimated for Kimama drill core basalts from a linear fit model using Ar/Ar ages and paleomagnetic ages. The onset and termination of paleomagnetic chrons and subchrons are shown by the small red dots, with normal polarity intervals demonstrated by gray shading. Ar/Ar ages are indicated by blue circles; the Adelaide Butte age is published in Kuntz et al. (2018) The youngest U-Pb ages of detrital zircon grains in the lower fluvial successions are 5.8 ± 0.13 Ma at 1749 m, and 6.2 ± 0.1 Ma at 1844 m depth (Potter, 2014); these ages (pink circles) are overlain on the linear fit projection to demonstrate concurrence with the 320 m/m.y. accumulation rate and indicate a depositional period of <100,000 years (modified from Champion and Duncan, 2012).

Downloaded from https://pubs.geoscienceworld.org/gsa/geosphere/article-pdf/doi/10.1130/GES01679.1/4663281/ges01679.pdf
by guest

elevation of the site prevented the incursion of water. Most loess deposits were deposited over hundreds to a few thousands of years.

Sources of rhyolite volcanism near the Kimama borehole are the Twin Falls and Picabo volcanic centers. To the west of the Kimama borehole, the Twin Falls volcanic center erupted between 10.5 and 8.5 Ma (Anders et al., 2009), well before initial basaltic volcanism in the Kimama region. The Picabo volcanic center is inferred to be located immediately to the east of the Kimama borehole and erupted between 10.4 and 6.6 Ma (Anders et al., 2009; Drew et al., 2013). Picabo volcanism waned after 6.6 Ma, after which volcanism migrated northeastward to the Heise volcanic center (6.6–4.4 Ma) (Bonnichsen et al., 2008; Anders et al., 2009). Although the Kimama drill core does not preserve silicic or mafic lavas within the age range of Picabo volcanism, volcanogenic zircons recovered from fluvial interbeds at 1749 and 1844 m depth yield four main statistical populations of ages: 7.1 ± 0.1 Ma, 6.9 ± 0.1 Ma, 6.2 ± 0.1 Ma, and 5.8 ± 0.1 Ma, which are generally coincident with eruptions of the Picabo and Heise fields (Potter, 2014). The bladed and euhedral nature of these volcanogenic zircons indicates an ash fall origin and minimal damage due to transport, suggesting they were mobilized, deposited, and buried by basalt soon after their eruption. Basaltic volcanism in the vicinity of the Kimama borehole was coeval with younger silicic eruptions from the Heise field, and it is likely that basaltic volcanism near the Kimama borehole initiated within a few million years after the cessation of silicic volcanism in the Picabo field, when heat flow and residual heat from the plume were likely relatively high.

CONCLUSIONS

The Kimama drill core is the most complete record of mafic volcanism and the construction of the CSRP over the past 5.8 m.y.; this record can help characterize and temporally characterize the volcanic history of the CSRP. Borehole stratigraphy, geochemistry, and paleomagnetic data demonstrate that volcanism at the Kimama drill site has been remarkably consistent over 5.8 m.y. A steady eruptive rate of flow units, flows, and flow groups, with minor volcanic hiatuses marked by sediment accumulation, have accumulated at a relatively stable rate of ~320 m/m.y.

Although the majority of flow groups are SROT, several Kimama flow groups display compositional variability consistent with differentiation cycles in the mafic mid-crustal sill. These cycles may be roughly constrained as occurring over ~77,000 years, close to the rate at which new flow groups erupt. Between monogenetic eruptive episodes, magma is fed into subvolcanic magma chambers from a network of stacked sill-like plutons where the assimilation of previously emplaced and partially crystalline magmas takes place, a process known as assimilation of consanguineous mafic intrusions (i.e., ACMI processes) (Potter et al., 2018).

The drill core samples a range of basalt super groups, flow groups, flows, flow units, and sediment interbeds. The thickness, age, facies characteristics, and geochemistry of basalts in the Kimama drill core support the inference that flow groups erupt over decadal time scales from small, shallow (2–4-km-depth) subvolcanic magma chambers with a unique geochemical signature; these chambers are typically associated with one vent. Relatively continuous basalt eruptive episodes in the vicinity of the Kimama borehole from 6.3 Ma through 0.48 Ma suggest that mantle heat flow was high enough to produce a steady supply of magma from the mid-crustal sill to the surface within ~2 m.y. of plume magmatism. In the aftermath of local plume magmatism and silicic volcanism, continuous high mantle heat flow in the Kimama region and the western SRP may be attributed to the thinning and channelization of the continental lithosphere along the plume track and the westward flow of magmas along the subcrustal lithospheric mantle gradient from the plume source (e.g., Hanan et al., 2008, Shervais and Hanan, 2008; Jean et al., 2014).

Additionally, subsurface geophysical data provide an accurate proxy to lithologic observations made from cored basalt and sediment. Individual basalt flow units, flows, flow groups (in the case of high–K-Fe flow groups), and sediment interbeds may be identified through the use of natural gamma-ray and neutron well log data. Combined with magnetostratigraphic and geochemical logging tools and geophysical logs, scientific drilling enables the interpretation of subsurface basalt flow group stratigraphy and the characterization of volcanic processes in young, underexposed volcanic provinces.

ACKNOWLEDGMENTS

This work was supported by U.S. Department of Energy award DE-EE0002848, by the International Continental Drilling Program (ICDP), and by a consortium of universities. This manuscript greatly benefitted from reviews by Matt Brueseke, Michael Petronis, and an anonymous reviewer. Discussions with Eric Christiansen, Paul Link, and the Hotspot Science Team (http://www.usu.edu/geo/shervais/Shervais-USU-Geology/Hotspot_Science_Team.html) were especially helpful, but any errors are our own.

REFERENCES CITED

Anders, M.H., Saltzman, J., and Hemming, S.R., 2009, Neogene tephra correlations in eastern Idaho and Wyoming Yellowstone for hotspot-related volcanism and tectonic activity: Geological Society of America Bulletin, v. 121, p. 837–856, https://doi.org/10.1130/B26300.1.

Anderson, S., and Lewis, B.D., 1989, Stratigraphy of the unsaturated zone at the radioactive waste management complex, Idaho National Engineering Laboratory, Idaho, U.S. Geological Survey.

Anderson, S.R., and Liszewski, M.J., 1997, Stratigraphy of the unsaturated zone and the Snake River Plain Aquifer at and near the Idaho National Engineering Laboratory, Idaho: U.S. Geological Survey Water-Resources Investigations Report 97-4183, 70 p., https://doi.org/10.2172/578514.

Anderson, S.R., Liszewski, M.J., and Cecil, L.D., 1997, Geologic ages and accumulation rates of basalt-flow groups and sedimentary interbeds in selected wells at the Idaho National Engineering Laboratory, Idaho: U.S. Geological Survey Water-Resources Investigations Report 97-4010, 43 p., https://doi.org/10.2172/481885.

Armstrong, R.L., Leeman, W.P., and Malde, H.E., 1975, K-Ar dating, Quaternary and Neogene rocks of the Snake River Plain, Idaho: American Journal of Science, v. 275, p. 225–251, https://doi.org/10.2475/ajs.275.3.225.

Baksi, A.K., 2007, A quantitative tool for detecting alteration in undisturbed rocks and minerals—I: Water, chemical weathering, and atmospheric argon, *in* Foulger, G.R., and Jurdy, D.M., eds., Plates, Plumes and Planetary Processes: Geological Society of America Special Paper 430, p. 285–303, https://doi.org/10.1130/2007.2430(15).

Beranek, L.P., Link, P.K., and Fanning, C.M., 2006, Miocene to Holocene landscape evolution of the western Snake River Plain region, Idaho: Using the SHRIMP detrital zircon provenance record to track eastward migration of the Yellowstone hotspot: Geological Society of America Bulletin, v. 118, no. 9–10, p. 1027–1050, https://doi.org/10.1130/B25896.1.

Downloaded from https://pubs.geoscienceworld.org/gsa/geosphere/article-pdf/doi/10.1130/GES01679.1/4663281/ges01679.pdf
by guest

Bonnichsen, B., and Godchaux, M.M., 2002, Late Miocene, Pliocene, and Pleistocene geology of southwestern Idaho with emphasis on basalts in the Bruneau-Jarbidge, Twin Falls, and western Snake River Plain regions: Tectonic and magmatic evolution of the Snake River Plain volcanic province: Idaho Geological Survey Bulletin, v. 30, p. 233–312.

Bonnichsen, B., Leeman, W.P., Honjo, N., McIntosh, W.C., and Godchaux, M.M., 2008, Miocene silicic volcanism in southwestern Idaho: Geochronology, geochemistry, and evolution of the central Snake River Plain: Bulletin of Volcanology, v. 70, no. 3, p. 315–342, https://doi.org/10.1007/s00445-007-0141-6.

Champion, D., and Duncan, R.A., 2012, Paleomagnetic and $^{40}Ar/^{39}Ar$ studies on tholeiite basalt samples from "HOTSPOT" corehole taken at Kimama, Idaho, central Snake River Plain: Washington, D.C., Eos (Transactions, American Geophysical Union), V13B-2842.

Champion, D.E., Lanphere, M.A., and Kuntz, M.A., 1988, Evidence for a new geomagnetic reversal from lava flows in Idaho: Discussion of short polarity reversals in the Brunhes and Late Matuyama Polarity Chrons: Journal of Geophysical Research, v. 93, no. B10, p. 11,677–11,680, https://doi.org/10.1029/JB093iB10p11667.

Champion, D.E., Lanphere, M.A., Anderson, S.R., and Kuntz, M.A., 2002, Accumulation and subsidence of late Pleistocene basaltic lava flows of the eastern Snake River Plain, Idaho, *in* Link, P.K., and Mink, L.L., eds., Geology, Hydrogeology, and Environmental Remediation: Idaho National Engineering and Environmental Laboratory, Eastern Snake River Plain, Idaho: Geological Society of America Special Paper 353, p. 175–192, https://doi.org/10.1130/0-8137-2353-1.175.

Champion, D.E., Hodges, M.K., Davis, L.C., and Lanphere, M.A., 2011, Paleomagnetic correlation of surface and subsurface basaltic lava flows and flow groups in the southern part of the Idaho National Laboratory, Idaho, with paleomagnetic data tables for drill cores: U.S. Geological Survey Scientific Investigations Report 2011-5049, 34 p.

Chitwood, L.A., 1994, Inflated basaltic lava—Examples of processes and landforms from central and southeast Oregon: Oregon Geology, v. 56, no. 1, p. 11–21.

Davis, L.C., Hannula, S.R., and Bowers, B., 1997, Procedures for use of, and drill cores and cuttings available for study at, the lithologic core storage library, Idaho National Engineering Laboratory, Idaho: U.S. Geological Survey Open-File Report 97-124 (DOE/ID-22135), 31 p.

Doherty, D.J., McBroome, L.A., and Kuntz, M.A., 1979, Preliminary geologic interpretation and lithologic log of the exploratory test well (INEL-1), Idaho National Engineering Laboratory, eastern Snake River Plain, Idaho: U.S. Geological Survey Open-File Report 79-1248, 10 p.

Drew, D.L., Bindeman, I.N., Watts, K.E., Schmitt, A.K., Fu, B., and McCurry, M., 2013, Crustal-scale recycling in caldera complexes and rift zones along the Yellowstone hotspot track: O and Hf isotopic evidence in diverse zircons from voluminous rhyolites of the Picabo volcanic field, Idaho: Earth and Planetary Science Letters, v. 381, p. 63–77, https://doi.org/10.1016/j.epsl.2013.08.007.

Duncan, R.A., and Hogan, L.G., 1994, Radiometric dating of young MORB using the ^{40}Ar-^{39}Ar incremental heating method: Geophysical Research Letters, v. 21, no. 18, p. 1927–1930, https://doi.org/10.1029/94GL01375.

Duncan, R.A., Hooper, P.R., Rehacek, J., Marsh, J.S., and Duncan, A.R., 1997, The timing and duration of the Karoo igneous event, southern Gondwana: Journal of Geophysical Research, v. 102, p. 18,127–18,138, https://doi.org/10.1029/97JB00972.

Goff, F., 1996, Vesicle cylinders in vapor-differentiated basalt flows: Journal of Volcanology and Geothermal Research, v. 71, no. 2–4, p. 167–185, https://doi.org/10.1016/0377-0273(95)00073-9.

Gradstein, F.M., Ogg, J.G., Schmitz, M.D., and Ogg, G.M., 2012, The Geologic Time Scale 2012: Elsevier, 1176 p., https://doi.org/10.1016/C2011-1-08249-8.

Greeley, R., 1977, Basaltic "plains" volcanism, *in* Greeley, R., and King, J.S., eds., Volcanism of the Eastern Snake River Plain, Idaho: A Comparative Planetary Guidebook: National Aeronautics and Space Administration, p. 23-44.

Greeley, R., 1982, The Snake River Plain, Idaho: Representative of a new category of volcanism: Journal of Geophysical Research, v. 87, B4, p. 2705–2712, https://doi.org/10.1029/JB087iB04p02705.

Hackett, W.R., and Smith, R.P., 1992, Quaternary volcanism, tectonics, and sedimentation in the Idaho National Engineering Laboratory area: Idaho Falls, Idaho, EG & G Services, Inc.

Hackett, W.R., Smith, R.P., and Khericha, S., 2004, Volcanic hazards of the Idaho National Engineering and Environmental Laboratory, southeast Idaho, *in* Bonnichsen, B., White, C.M., and McCurry, M., eds., Tectonic and Magmatic Evolution of the Snake River Plain Volcanic Province: Idaho Geological Survey Bulletin 30, p. 461–482.

Hanan, B.B., Shervais, J.W., and Vetter, S.K., 2008, Yellowstone plume–continental lithosphere interaction beneath the Snake River Plain: Geology, v. 36, p. 51–54, https://doi.org/10.1130/G23935A.1.

Hodges, M.K., Link, P.K., and Fanning, C.M., 2009, The Pliocene Lost River found to west: Detrital zircon evidence of drainage disruption along a subsiding hotspot track: Journal of Volcanology and Geothermal Research, v. 188, no. 1, p. 237–249, https://doi.org/10.1016/j.jvolgeores.2009.08.019.

Hon, K., Kauahihaua, J., Denlinger, R., and McKay, K., 1994, Emplacement and inflation of pahoehoe sheet flows: Observations and measurements of active lava flows on Kilauea Volcano, Hawaii: Geological Society of America Bulletin, v. 106, p. 351–370, https://doi.org/10.1130/0016-7606(1994)106<0351:EAIOPS>2.3.CO;2.

Huang, H.-H., Lin, F.-C., Schmandt, B., Farrell, J., Smith, R.B., and Tsai, V.C., 2015, The Yellowstone magmatic system from the mantle plume to the upper crust: Science, v. 348, no. 6236, p. 773–776, https://doi.org/10.1126/science.aaa5648.

Hughes, S.S., Smith, R.P., Hackett, W.R., and Anderson, S.R., 1999, Mafic volcanism and environmental geology of the eastern Snake River Plain, Idaho, *in* Hughes, S.S., and Thackray, G.D., Guidebook to the Geology of Eastern Idaho: Idaho Museum of Natural History, p. 143–168.

Hughes, S.S., Wetmore, P.H., and Casper, J.L., 2002, Evolution of Quaternary tholeiitic basalt eruptive centers on the eastern Snake River Plain, Idaho, *in* Bonnichsen, B., White, C.M., and McCurry, M., eds., Tectonic and Magmatic Evolution of the Snake River Plain Volcanic Province: Idaho Geological Survey Bulletin 30, p. 363–385.

Jean, M.M., Shervais, J.W., Champion, D.E., and Vetter, S.K., 2013, Geochemical and paleomagnetic variations in basalts from the Wendell Regional Aquifer Systems Analysis (RASA) drill core: Evidence for magma recharge and assimilation–fractional crystallization from the central Snake River Plain, Idaho: Geosphere, v. 9, no. 5, p. 1319–1335, https://doi.org/10.1130/GES00914.1.

Jean, M.M., Hanan, B.B., and Shervais, J.W., 2014, Yellowstone hotspot–continental lithosphere interaction: Earth and Planetary Science Letters, v. 389, p. 119–131, https://doi.org/10.1016/j.epsl.2013.12.012.

Jean, M.M., Christiansen, E.H., Champion, D.E., Vetter, S.K., Phillips, W.M., Schuth, S., and Shervais, J.W., 2018, Caldera life-cycles of the Yellowstone Hotspot Track: Death and rebirth of the Heise Caldera: Journal of Petrology, v. 59, p. 1643–1670, https://doi.org/10.1093/petrology/egy074.

Kessler, J.A., Bradbury, K., Evans, J., Pulsipher, M., Schmitt, D., Shervais, J., Rowe, F., and Varriale, J., 2017, Geology and in situ stress of the MH-2 borehole, Idaho, USA: Insights into western Snake River Plain structure from geothermal exploration drilling: Lithosphere, v. 9, p. 476-498, https://doi.org/10.1130/L609.1.

Knott, T.R., Branney, M.J., Reichow, M.K., Finn, D.R., Coe, R.S., Storey, M., Barfod, D., and McCurry, M., 2016, Mid-Miocene record of large-scale Snake River–type explosive volcanism and associated subsidence on the Yellowstone hotspot track: The Cassia Formation of Idaho, USA: Geological Society of America Bulletin, v. 128, p. 1121–1146, https://doi.org/10.1130/B31324.1.

Koppers, A.A.P., 2002, ArArCALC—software for $^{40}Ar/^{39}Ar$ age calculations: Computers & Geosciences, v. 28, p. 605–619, https://doi.org/10.1016/S0098-3004(01)00095-4.

Koppers, A.A.P., Staudigel, H., and Wijbrans, J.R., 2000, Dating crystalline groundmass separates of altered Cretaceous seamount basalts by the $^{40}Ar/^{39}Ar$ incremental heating technique: Chemical Geology, v. 166, no. 1–2, p. 139–158, https://doi.org/10.1016/S0009-2541(99)00188-6.

Kuntz, M., Covington, H., and Schorr, L., 1992, An overview of basaltic volcanism of the eastern Snake River Plain, Idaho, *in* Link, P.K., Kuntz, M.A., and Platt, L.P., eds., Regional Geology of Eastern Idaho and Western Wyoming: Geological Society of America Memoir 179, p. 227–268, https://doi.org/10.1130/MEM179-p227.

Kuntz, M.A., 1978, Geology of the Arco-Big Southern Butte area, eastern Snake River Plain, and potential volcanic hazards to the radioactive waste management complex, and other waste storage and reactor facilities at the Idaho National Engineering Laboratory, Idaho with a section on statistical treatment of the age of lava flows *by* John O. Kork: U.S. Geological Survey Open-File Report 78-691, 70 p.

Kuntz, M.A., Champion, D.E., Spiker, E.C., and Lefebvre, R.H., 1986, Contrasting magma types and steady-state, volume-predictable, basaltic volcanism along the Great Rift, Idaho: Geological Society of America Bulletin, v. 97, no. 5, p. 579–594, https://doi.org/10.1130/0016-7606(1986)97<579:CMTASV>2.0.CO;2.

Kuntz, M.A., Anderson, S.R., Champion, D.E., Lanphere, M.A., and Grunwald, D.J., 2002, Tension cracks, eruptive fissures, dikes, and faults related to late Pleistocene–Holocene basaltic volcanism and implications for the distribution of hydraulic conductivity in the eastern Snake River Plain, in Idaho, *in* Link, P.K., and Mink, L.L., eds., Geology, Hydrogeology, and Environmental Remediation: Idaho National Engineering and Environmental Laboratory, eastern Snake River Plain, Idaho: Geological Society of America Special Paper 353, p. 111–133, https://doi.org/10.1130/0-8137-2353-1.111.

Downloaded from https://pubs.geoscienceworld.org/gsa/geosphere/article-pdf/doi/10.1130/GES01679.1/4663281/ges01679.pdf
by guest

Kuntz, M.A., Skipp, B., Champion, D.E., Gans, P.B., Van Sistine, D.P., and Snyders, S.R., 2007, Geologic Map of the Craters of the Moon 30′ × 60′ Quadrangle, Idaho: U.S. Geological Survey Scientific Investigations Map 2969, 64 p., pamphlet, 1 plate, scale 1:100,000, https://doi.org/10.3133/sim2969.

Kuntz, M.A., Champion, D.E., Turrin, B.R., Gans, P.B., Covington, H.R., and Van Sistine, D.P., 2018, Geologic Map of the North Half of the Lake Walcott 30′ × 60′ Quadrangle, Idaho, U.S. Geologic Survey Scientific Investigations Report 3405, pamphlet 25 p., scale 1:100,000, https://doi.org/10.3133/sim3405.

Lachmar, T.E., Freeman, T.G., Sant, C.J., Walker, J.R., et al., 2017, Effect of an 860-m thick, cold, freshwater aquifer on geothermal potential along the axis of the eastern Snake River Plain, Idaho: Geothermal Energy, v. 5, p. 28, https://doi.org/10.1186/s40517-017-0086-8.

Leeman, W.P., 1982, Evolved and hybrid lavas from the Snake River Plain, Idaho, *in* Bonnichsen, B., and Breckenridge, R.M., eds., Cenozoic Geology of Idaho: Idaho Bureau of Mines and Geology Bulletin 26, p. 181–191.

Lindholm, G.F., 1996, Summary of the Snake River regional aquifer system analysis in Idaho and eastern Oregon: U.S. Geological Survey Professional Paper 1408-A, 59 p, https://doi.org/10.3133/pp1408A.

McFadden, P.L., and Reid, A.B., 1982, Analysis of palaeomagnetic inclination data: Geophysical Journal International, v. 69, no. 2, p. 307–319, https://doi.org/10.1111/j.1365-246X.1982.tb04950.x.

Morgan, W.J., 1972, Plate motions and deep mantle convection, *in* Shagam, R., Hargraves, R.B., Morgan, W.J., Van Houten, F.B., Burk, C.A., Holland, H.D., and Hollister, L.C., eds., Studies in Earth and Space Sciences: Geological Society of America Memoir 132, p. 7–22, https://doi.org/10.1130/MEM132-p7.

Morse, L.H., and McCurry, M., 2002, Genesis of alteration of Quaternary basalts within a portion of the eastern Snake River Plain aquifer, *in* Link, P.K., and Mink, L.L., eds., Geology, Hydrogeology, and Environmental Remediation: Idaho National Engineering and Environmental Laboratory, Eastern Snake River Plain, Idaho: Geological Society of America Special Paper 353, p. 213–224, https://doi.org/10.1130/0-8137-2353-1.213.

Nier, A.O., 1950, A redetermination of the relative abundances of the isotopes of carbon, nitrogen, oxygen, argon, and potassium: Physical Review, v. 77, p. 789–793, https://doi.org/10.1103/PhysRev.77.789.

Peng, X., and Humphreys, E.D., 1998, Crustal Velocity Structure Across the eastern Snake River Plain and Yellowstone Swell: Journal of Geophysical Research, v. 103, no. B4, p. 7171–7186, https://doi.org/10.1029/97JB03615.

Pierce, K.L., and Morgan, L.A., 1992, The track of the Yellowstone Hotspot: Volcanism, faulting, and uplift, *in* Link, P.K., Kuntz, M.A., and Platt, L.B., eds., Regional Geology of Eastern Idaho and Western Wyoming: Geological Society of America Memoir 179, p. 1–54, https://doi.org/10.1130/MEM179-p1.

Pierce, K.L., and Morgan, L.A., 2009, Is the track of the Yellowstone hotspot driven by a deep mantle plume?—Review of volcanism, faulting, and uplift in light of new data: Journal of Volcanology and Geothermal Research, v. 188, p. 1–25, https://doi.org/10.1016/j.jvolgeores.2009.07.009.

Potter, K.E., 2014, The Kimama Core: A 6.4 Ma Record of Volcanism, Sedimentation, and Magma Petrogenesis on the Axial Volcanic High, Snake River Plain, ID [Ph.D. dissertation]: Logan, Utah, Utah State University, 161 p.

Potter, K.E., Shervais, J.W., Christiansen, E.H., and Vetter, S.K., 2018, Evidence for cyclical fractional crystallization, recharge, and assimilation in basalts of the Kimama Drill Core, central Snake River Plain, Idaho: 5.5-million-years of petrogenesis in a mid-crustal sill complex: Frontiers of Earth Science, v. 6, 17 p.

Putirka, K.D., Kuntz, M.A., Unruh, D.M., and Vaid, N., 2009, Magma evolution and ascent at the Craters of the Moon and neighboring volcanic fields, southern Idaho, USA: Implications for the evolution of polygenetic and monogenetic volcanic fields: Journal of Petrology, v. 50, no. 9, p. 1639–1665, https://doi.org/10.1093/petrology/egp045.

Renne, P.R., Swisher, C.C., Deino, A.L., Karner, D.B., Owens, T., and DePaolo, D.J., 1998, Intercalibration of standards, absolute ages and uncertainties in $^{40}Ar/^{39}Ar$ dating: Chemical Geology. Isotope Geoscience Section, v. 145, p. 117–152.

Sant, C.J., 2013, Geothermal alteration of basaltic core from the Snake River Plain, Idaho: [M.S. thesis]: Logan, Utah, Utah State University, 113 p.

Sant, C.J., and Shervais, J.W., 2011, Project Hotspot: Preliminary analysis of secondary mineralization in basaltic core, central Snake River Plain: Geothermal Resources Council Transactions, v. 35, p. 987–989.

Self, S., Keszthelyi, L., and Thordarson, T., 1998, The importance of pahoehoe: Annual Review of Earth and Planetary Sciences, v. 26, p. 81–110, https://doi.org/10.1146/annurev.earth.26.1.81.

Shervais, J.W., and Hanan, B.B., 2008, Lithospheric topography, tilted plumes, and the track of the Snake River–Yellowstone hot spot: Tectonics, v. 27, https://doi.org/10.1029/2007TC002181.

Shervais, J., Vetter, S., and Hackett, W., 1994, Chemical stratigraphy of basalts in coreholes NPR-E and WO-2, Idaho National Engineering Laboratory, Idaho: Implications for plume dynamics in the Snake River Plain: Santa Fe, New Mexico, Proceedings of the VII International Symposium on the Observation of Continental Crust through Drilling, p. 93–96.

Shervais, J.W., Vetter, S.K., and Hanan, B.B., 2006, Layered mafic sill complex beneath the eastern Snake River Plain: Evidence from cyclic geochemical variations in basalt: Geology, v. 34, p. 365–368, https://doi.org/10.1130/G22226.1.

Shervais, J.W., Evans, J.P., Christiansen, E.J., Schmitt, D.R., Kessler, J.A., Potter, K.E., Jean, M.M., Sant, C.J., and Freeman, T.G., 2011, Project Hotspot—The Snake River Scientific Drilling Project: Geothermal Resources Council Transactions, v. 35, p. 995–1003.

Shervais, J.W., Nielson, D.L., Evans, J.P., Christensen, E.J., Morgan, L., Shanks, W.C., Delahunty, C., Schmitt, D.R., Liberty, L.M., Blackwell, D.D., Glenn, J.M., Kessler, J.E., Potter, K.E., Jean, M.M., Sant, C.J., and Freeman, T.G., 2012, Hotspot: The Snake River geothermal drilling project—Initial report: Geothermal Resources Council Transactions, v. 36, p. 767–772.

Shervais, J.W., Schmitt, D.R., Nielson, D., Evans, J.P., Christiansen, E.H., Morgan, L., Kessler, J.A., Morgan, L.A., Prokopenko, A.A., Liberty, L.M., and Glen, J.M.G., 2013, First Results from HOTSPOT: The Snake River Plain Scientific Drilling Project, Idaho, U.S.A: Scientific Drilling, v. 15, p. 36–45, https://doi.org/10.5194/sd-15-36-2013.

Shervais, J.W., Evans, J.P., Schmitt, D.R., Christiansen, E.H., and Prokopenko, A., 2014, Drilling into the track of the Yellowstone hot spot: Eos [Transactions, American Geophysical Union], v. 95, no. 10, p. 85–86.

Smith, R.B., and Braile, L.W., 1994, The Yellowstone hotspot: Journal of Volcanology and Geothermal Research, v. 61, p. 121–187, https://doi.org/10.1016/0377-0273(94)90002-7.

Smith, R.B., Jordan, M., Steinberger, B., Puskas, C.M., Farrell, J., Waite, G.P., Husen, S., Chang, W.L., and O'Connell, R., 2009, Geodynamics of the Yellowstone hotspot and mantle plume: Seismic and GPS imaging, kinematics, and mantle flow: Journal of Volcanology and Geothermal Research, v. 188, no. 1–3, p. 26–56, https://doi.org/10.1016/j.jvolgeores.2009.08.020.

Smith, R.E., 1967, Segregation vesicles in basaltic lava: American Journal of Science, v. 265, no. 8, p. 696–713, https://doi.org/10.2475/ajs.265.8.696.

Steiger, R.H., and Jäger, E., 1977, Subcommission on geochronology: Convention on the use of decay constants in geo- and cosmochronology: Earth and Planetary Science Letters, v. 36, p. 359–362, https://doi.org/10.1016/0012-821X(77)90060-7.

Twining, B.V., and Bartholomay, R.C., 2011, Geophysical logs and water-quality data collected for boreholes Kimama-1A and-1B, and a Kimama water supply well near Kimama, southern Idaho: U.S. Geological Survey Data Series 622 (DOE/ID 22215), 18 p., plus appendix.

Twining, B.V., Hodges, M.K., and Orr, S.M., 2008, Construction diagrams, geophysical logs, and lithologic descriptions for boreholes USGS 126a, 126b, 127, 128, 129, 130, 131, 132, 133, and 134, Idaho National Laboratory, Idaho: U.S. Geological Survey Digital Series 350, 26 p.

Waite, G.P., Smith, R.B., and Allen, R.M., 2006, VP and VS structure of the Yellowstone hot spot from teleseismic tomography: Evidence for an upper mantle plume: Journal of Geophysical Research. Solid Earth, v. 111, B4, 21 p.

Walker, G.P.L., 1971, Compound and simple lava flows and flood basalts: Bulletin Volcanologique, v. 35, p. 579–590, https://doi.org/10.1007/BF02596829.

Walker, G.P.L., 1991, Structure, and origin by injection of lava under surface crust, of tumuli, "lava rises", "lava-rise pits" and "lava-inflation clefts" in Hawaii: Bulletin of Volcanology, v. 53, p. 546–558, https://doi.org/10.1007/BF00298155.

Walker, G.P.L., 1993, Basaltic-volcano systems, *in* Prichard, H.M., Alabaster, T., Harris, N.B.W., and Neary, C.R., eds., Magmatic Processes and Plate Tectonics: Geological Society of London Special Publication 76, p. 3–38, https://doi.org/10.1144/GSL.SP.1993.076.01.01.

Welhan, J.A., Johannesen, C.M., Reeves, K.S., Clemo, T.M., Glover, J.A., and Bosworth, K.W., 2002, Morphology of inflated pahoehoe lavas and spatial architecture of their porous and permeable zones, eastern Snake River Plain, Idaho, *in* Link, P.K., and Mink, L.L., eds., Geology, Hydrogeology, and Environmental Remediation: Idaho National Engineering and Environmental Laboratory, Eastern Snake River Plain, Idaho: Geological Society of America Special Paper 353, p. 135–150, https://doi.org/10.1130/0-8137-2353-1.135.

Downloaded from https://pubs.geoscienceworld.org/gsa/geosphere/article-pdf/doi/10.1130/GES01679.1/4663281/ges01679.pdf
by guest